

Effective lattice model for collective modes in a Fermi liquid with spin-orbit coupling

Abhishek Kumar^{1,*} and Dmitrii L. Maslov¹

¹*Department of Physics, University of Florida, Gainesville, Florida, 32611*

(Dated: December 3, 2024)

A Fermi-liquid (FL) with spin-orbit coupling (SOC) supports a special type of collective modes—spin-chiral waves—which are oscillations of magnetization even in the absence of the external magnetic field. In this work, we study the collective spin modes of a two-dimensional (2D) FL in the presence of both SOC (of Rashba and Dresselhaus type) and in-plane magnetic field. We map the system of coupled kinetic equations for the angular harmonics of the distribution function onto an effective one-dimensional tight-binding model, in which the lattice sites correspond to values of the angular momentum. Linear-in-momentum coupling ensures that the effective tight-binding model has only nearest-neighbor hopping. In this language, the continuum of spin-flip excitations becomes a lattice band. The FL interaction, characterized by the harmonics of the Landau function, is mapped on effective disorder of both on-site and bond type. The collective modes correspond to bound states produced by the disorder. We find the dispersions of the collective modes both analytically, for the case when the Landau function can be approximated by up to the first harmonic, and numerically for the most general case.

PACS numbers: 78.67.-n, 78.20.Bh, 73.50.Gr, 73.50.Gd

Contents		
I. Introduction	1	4. Competition between three on-site impurities and two defect bonds 17
II. Model and formalism	2	B. Collective modes for interaction in $m = 0$ channel within tight-binding formalism 18
III. Quantum kinetic equation as an effective lattice model	4	C. Interaction in $m = 0$ and $m = 1$ harmonic channel 18
IV. Effective lattice model with Rashba coupling only	5	References 20
V. Partially-polarized Fermi liquid with Rashba spin-orbit coupling	5	
A. Non-interacting case	5	
B. Interacting case	7	
C. s -wave approximation for the Landau function	8	
1. Exact solution of the equations of motion.	8	
2. Physical interpretation within the effective lattice model	9	
D. Beyond s -wave approximation for the Landau function	13	
VI. A Fermi liquid with Rashba and Dresselhaus spin-orbit coupling	13	
VII. Conclusions	14	
A. One-dimensional tight-binding model with impurities and bond defects	15	
1. On-site disorder	15	
2. Bond disorder	16	
3. Competition between on-site disorder and bond disorder	16	

I. Introduction

Spintronics is the study of the properties of electron gas in the presence of spin-orbit coupling (SOC). In systems with SOC, the electronic spin couples to an external electric field $\tilde{\mathbf{E}}$, generated either from dc current or electromagnetic wave, which provides them a non-zero drift momentum. The electron system as a whole thus experiences an effective magnetic field. This famous phenomena is called electron spin resonance (ESR) spectroscopy due to SOC.¹ Now a days ESR has become an invaluable tool to study the dynamics of electronic spin.^{2–4} This process is advantageous over conventional or direct ESR; ESR in the presence of an external magnetic field, in the sense that the signal intensity one observes is significantly strong. In 2DEG with static in-plane magnetic field, the only resonant feature is due to a pole in the spin susceptibility at the Larmor frequency. However, because the spin susceptibility is proportional to $1/c^2$, where c is the speed of light, the direct ESR signal is very weak. SOC here changes the situation drastically by producing an effective magnetic field, which acts on electron spins. To make the ESR signal even stronger the magnitude of bare SOC can be strongly enhanced by virtual interband transitions.⁵ This results in coupling of electronic spin to

the electric component of electromagnetic wave stronger as compared to that to the magnetic one. The effect is called electric dipole spin resonance (EDSR),^{6–8} which gives rise to a range of spectacular phenomena.

As of now, most of the ESR and EDSR experiments are interpreted in terms of the single-particle picture outlined above. In the recent article⁹, it is however shown that the single particle phenomena is not generic to ESR. In the case of two-dimensional Fermi liquid (FL) with spin-orbit coupling (SOC), many-body correlations play an interesting role. In the presence of an in-plane magnetic field, depending on whether the magnetic field is below or above the critical value, there can be up to three spin-chiral collective modes, augmented by the Silin-Leggett mode.^{10,11} In all of the above cases, the electron-electron interaction (*eei*) is treated perturbatively. To the best of our knowledge no one has so far considered the case of non-perturbative *eei* in this type of system. We make an attempt to solve this problem by considering the system effective on a 1D lattice. The goal of this article is two-fold. First we discuss the tight-binding approach to FL theory of ESR and second the effect of electron-electron interaction (*eei*) on ESR in the non-perturbative limit. Starting from the phenomenological FL equations, we derived the equations of motion for the deviation of occupation number at $q = 0$ for any arbitrary interaction and observed that this system can be mapped to the 1D lattice model with nearest-neighbor as the most significant interaction. We emphasize that this mapping is unique to the two-dimensional system with SOC in the presence of magnetic field; absence of either of these two violates this theory. We prove our prediction with explicit calculation by making appropriate transformations in the equation of motion. We first reproduce the RPA result for interaction in just one angular harmonic channel⁹ using tight-binding formalism and then generalize our result for interaction in any arbitrary channel. Although, the exact solution for any arbitrary interaction is not possible, using tight-binding formalism one can atleast correctly predict the spectrum of bound states. For the sake of completeness, we provide numerical solution for this case by assuming any reasonable form of interaction.

II. Model and formalism

We study a 2D FL in the presence of spin-orbit coupling (SOC) of both Rashba^{12,13} and Dresselhaus¹⁴ types, and an in-plane static magnetic field. For the (001) surface of a cubic crystal, the single-particle part of the Hamiltonian reads

$$\hat{H}_0 = \frac{\mathbf{p}^2}{2m_b} \hat{\sigma}_0 + \alpha (\hat{\sigma}_1 p_2 - \hat{\sigma}_2 p_1) + \beta (\hat{\sigma}_1 p_2 + \hat{\sigma}_2 p_1) + \frac{g\mu_B}{2} \hat{\sigma}_1 B, \quad (1)$$

where m_b is the band mass, $\hat{\sigma}_{1,2,3}$ are the Pauli matrices, $\hat{\sigma}_0$ is the 2×2 identity matrix, α (β) is the Rashba (Dresselhaus) coupling constant, μ_B is the Bohr magneton, g

is the Landé factor, and B is the magnetic field. Furthermore, indices $1 \dots 3$ label the axes of a Cartesian system with the x_1 and x_2 axes chosen to be along the $[1\bar{1}0]$ and $[110]$ directions, respectively, see Fig. 1. The magnetic field is chosen to be along the high-symmetry axis (x_1). If the Dresselhaus term is absent ($\beta = 0$), the system is invariant with respect to rotations about the x_3 -axis. In this case, the direction of \mathbf{B} is arbitrary, and the x_1 -axis can be chosen along this direction.

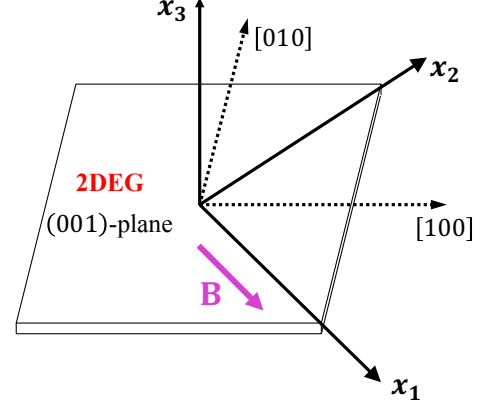


FIG. 1. Square lattice with rotated coordinate frame. In the standard coordinate frame of a (001) surface of a cubic crystal, $[100]$ and $[010]$ denotes x and y axes, respectively. Upon rotation by $\pi/4$ about the axis perpendicular to the plane in the clockwise direction (x_3), these axes point along $[1\bar{1}0]$ and $[110]$ directions, respectively: denoted by x_1 and x_2 . The magnetic field is chosen to be along the high-symmetry axis (x_1) in the new frame.

We assume that both SOC and magnetic field are weak, in a sense that the corresponding energy scales are small compared to the Fermi energy. In this case, one can neglect the effect of these perturbations on the Landau interaction function,^{9,15,16} which retains its $SU(2)$ -invariant form:

$$\nu_F f_{\alpha\beta,\gamma\delta}(\theta_{\mathbf{p}\mathbf{p}'}) = F^s(\theta_{\mathbf{p}\mathbf{p}'}) \delta_{\alpha\gamma} \delta_{\beta\delta} + F^a(\theta_{\mathbf{p}\mathbf{p}'}) \hat{\sigma}_{\alpha\gamma} \cdot \hat{\sigma}_{\beta\delta}, \quad (2)$$

where $\theta_{\mathbf{p}\mathbf{p}'} = \theta_{\mathbf{p}} - \theta_{\mathbf{p}'}$, $\theta_{\mathbf{k}}$ is the azimuthal angle of vector \mathbf{k} , and $\nu_F = m^*/\pi = m_b(1 + F_1^s)/\pi$ is the renormalized density of states. Only the spin-dependent part of the Landau interaction function will be important for what follows. Note that crystalline anisotropy enters only via the Dresselhaus term in Hamiltonian (1), whereas the underlying FL is considered as rotationally-invariant.

Both SOC and magnetic field will be treated as weak external forces imposed on an $SU(2)$ -invariant FL. The self-consistent equation for the variation of the quasiparticle energy reads

$$\delta\hat{\varepsilon}(\mathbf{p}) = \delta\hat{\varepsilon}_s(\mathbf{p}) + \text{Tr}' \int \frac{d^2 p'}{(2\pi)^2} \hat{f}_{\mathbf{p}\mathbf{p}'} \delta\hat{n}(\mathbf{p}'), \quad (3)$$

where $'$ indicates the spin state of the quasiparticle with momentum \mathbf{p}' , $\delta\hat{n}(\mathbf{p})$ is the variation of the occupation

number, and

$$\delta\hat{\varepsilon}_s(\mathbf{p}) = \frac{1}{2}\Delta_R(e_2\hat{\sigma}_1 - e_1\hat{\sigma}_2) + \frac{1}{2}\Delta_D(e_2\hat{\sigma}_1 + e_1\hat{\sigma}_2) + \frac{1}{2}\Delta_Z\hat{\sigma}_1 \quad (4)$$

is the variation of the quasiparticle energy due to SOC of both Rashba and Dresselhaus types and external magnetic field. Here $\Delta_R = 2\alpha p_F$, $\Delta_D = 2\beta p_F$, and $\Delta_Z = g\mu_B B$ are the spin-orbit and Zeeman energy splittings, respectively, and $\mathbf{e} = \mathbf{p}/p$. (We choose Δ_Z to be non-negative, whereas Δ_R and Δ_D can be of either sign.) In equilibrium, Eq. (3) is solved by an Ansatz $\delta\hat{\varepsilon}(\mathbf{p}) = \delta\hat{\varepsilon}_s^*(\mathbf{p})$ and $\delta\hat{n}(\mathbf{p}) = \partial_\varepsilon n_0 \delta\hat{\varepsilon}_s^*(\mathbf{p})$, where n_0 is the Fermi function and $\delta\hat{\varepsilon}_s^*(\mathbf{p})$ differs from $\delta\hat{\varepsilon}_s(\mathbf{p})$ in Eq. (4) only in that the bare energy splittings are replaced by the renormalized ones. Expanding $F^a(\theta)$ in a series of 2D harmonics,

$$F^a(\theta) = \sum_m F_m^a e^{im\theta} \quad (5)$$

we obtain the renormalized energy splittings as^{9,15,17}

$$\begin{aligned} \Delta_R^* &= \frac{\Delta_R}{1 + F_1^a}, \quad \Delta_D^* = \frac{\Delta_D}{1 + F_1^a}, \\ \Delta_Z^* &= \frac{\Delta_Z}{1 + F_0^a}. \end{aligned} \quad (6)$$

In general, each type of SOC coupling is parametrized by two energies, e.g., the spin-orbit splitting, $\Delta_R = 2\alpha k_F$, and the Rashba energy, $E_R = m_b\alpha^2/2$ for the Rashba case, and similarly for the Dresselhaus SOC. However,

since we assumed SOC to be weak, the Rashba (Dresselhaus) energy, which is quadratic in α (β) will not show up in our theory.

Now we are set to derive equations describing the collective modes of our system. It is convenient to introduce a set of rotated Pauli matrices¹⁵

$$\tau^1(\mathbf{p}) = -\sigma_3, \quad \tau^2(\mathbf{p}) = \mathbf{e} \cdot \boldsymbol{\sigma}, \quad \text{and} \quad \tau^3(\mathbf{p}) = e_2\hat{\sigma}_1 - e_1\hat{\sigma}_2, \quad (7)$$

and decompose $\delta\hat{n}(\mathbf{p})$ into the equilibrium and non-equilibrium parts as

$$\delta\hat{n}(\mathbf{p}, t) = \partial_\varepsilon n_0 [\delta\hat{\varepsilon}_s^*(\mathbf{p}) + \mathbf{u}(\theta_{\mathbf{p}}, t) \cdot \hat{\boldsymbol{\tau}}], \quad (8)$$

where vector $\mathbf{u}(\theta_{\mathbf{p}}, t)$ parametrizes the non-equilibrium part of the occupation number. In a spatially-uniform case and in the absence of the residual interaction between quasiparticles, the occupation number satisfies the quantum kinetic equation

$$i \frac{\partial \delta\hat{n}(\mathbf{p}, t)}{\partial t} = [\delta\hat{\varepsilon}(\mathbf{p}, t), \delta\hat{n}(\mathbf{p}, t)]. \quad (9)$$

This seemingly simple equation embodies complex quantum dynamics and, as will be shown below, allows for a transparent interpretation in terms of the effective lattice model. Substituting $\delta\hat{n}(\mathbf{p})$ from Eq. (8) and $\delta\hat{\varepsilon}(\mathbf{p})$ from Eq. (3) into Eq. (9), and linearizing with respect to \mathbf{u} , we obtain

$$\begin{aligned} i\partial_t \mathbf{u} \cdot \hat{\boldsymbol{\tau}} &= [\delta\hat{\varepsilon}_s^*, \text{Tr}' \int_{\theta_{\mathbf{p}'}} F^a(\theta_{\mathbf{p}\mathbf{p}'}) (\hat{\boldsymbol{\sigma}} \cdot \hat{\boldsymbol{\sigma}}') (\mathbf{u}' \cdot \hat{\boldsymbol{\tau}}')] \\ &\quad + [\delta\hat{\varepsilon}_s^*, \mathbf{u} \cdot \hat{\boldsymbol{\tau}}], \end{aligned} \quad (10)$$

where $\delta\hat{\varepsilon}_s^* \equiv \delta\hat{\varepsilon}_s^*(\mathbf{p})$, $\mathbf{u} \equiv \mathbf{u}(\theta_{\mathbf{p}}, t)$, $\mathbf{u}' \equiv \mathbf{u}(\theta_{\mathbf{p}'}, t)$, $\hat{\boldsymbol{\tau}}' \equiv \hat{\boldsymbol{\tau}}'(\mathbf{p})$, and $\int_{\theta_{\mathbf{k}}} \equiv \int (d\theta_{\mathbf{k}}/2\pi)$. Using the identities $\hat{\boldsymbol{\sigma}} \cdot \text{Tr}(\hat{\boldsymbol{\sigma}}\hat{\tau}'_i) = 2\tau'_i$ and $[\hat{\tau}_3, \hat{\tau}'_2] = -2i\hat{\tau}_1 \cos\theta_{\mathbf{p}\mathbf{p}'}$,¹⁵ we find that the components of vector $\mathbf{u}(\theta_{\mathbf{p}}, t)$ satisfy the following system of equations

$$\begin{aligned} \frac{\partial u_1(\theta_{\mathbf{p}})}{\partial t} &= -[\Delta_R^* + \Delta_Z^* \sin\theta_{\mathbf{p}} - \Delta_D^* \cos 2\theta_{\mathbf{p}}] u_2(\theta_{\mathbf{p}}) + [\Delta_Z^* \cos\theta_{\mathbf{p}} + \Delta_D^* \sin 2\theta_{\mathbf{p}}] u_3(\theta_{\mathbf{p}}) \\ &\quad - \int_{\theta_{\mathbf{p}'}} F^a(\theta_{\mathbf{p}\mathbf{p}'}) [\Delta_R^* \cos(\theta_{\mathbf{p},\mathbf{p}'} + \Delta_Z^* \sin\theta_{\mathbf{p}'} - \Delta_D^* \cos(\theta_{\mathbf{p}} + \theta_{\mathbf{p}'})) u_2(\theta_{\mathbf{p}'}) \\ &\quad + \int_{\theta_{\mathbf{p}'}} F^a(\theta_{\mathbf{p}\mathbf{p}'}) [\Delta_R^* \sin(\theta_{\mathbf{p},\mathbf{p}'} + \Delta_Z^* \cos\theta_{\mathbf{p}'} + \Delta_D^* \sin(\theta_{\mathbf{p}} + \theta_{\mathbf{p}'})) u_3(\theta_{\mathbf{p}'}), \end{aligned} \quad (11a)$$

$$\frac{\partial u_2(\theta_{\mathbf{p}})}{\partial t} = [\Delta_R^* + \Delta_Z^* \sin\theta_{\mathbf{p}} - \Delta_D^* \cos 2\theta_{\mathbf{p}}] u_1(\theta_{\mathbf{p}}) + [\Delta_R^* + \Delta_Z^* \sin\theta_{\mathbf{p}} - \Delta_D^* \cos 2\theta_{\mathbf{p}}] \int_{\theta_{\mathbf{p}'}} F^a(\theta_{\mathbf{p}\mathbf{p}'} u_1(\theta_{\mathbf{p}'}), \quad (11b)$$

$$\frac{\partial u_3(\theta_{\mathbf{p}})}{\partial t} = -[\Delta_Z^* \cos\theta_{\mathbf{p}} + \Delta_D^* \sin 2\theta_{\mathbf{p}}] u_1(\theta_{\mathbf{p}}) - [\Delta_Z^* \cos\theta_{\mathbf{p}} + \Delta_D^* \sin 2\theta_{\mathbf{p}}] \int_{\theta_{\mathbf{p}'}} F^a(\theta_{\mathbf{p}\mathbf{p}'} u_1(\theta_{\mathbf{p}'}). \quad (11c)$$

[From now on, the argument t of $\mathbf{u}(\theta_{\mathbf{k}}, t)$ will be sup-

pressed.] At the next step, we expand \mathbf{u} and F^a over a

basis of angular harmonics [$\mathbf{u} = \sum_m e^{im\theta} \mathbf{u}^m$ and $F^a(\theta) = \sum_m e^{im\theta} F_m^a$] to obtain

$$\begin{aligned} \frac{\partial u_1^m}{\partial t} = & -\Delta_R^* u_2^m \left[1 + \frac{1}{2}(F_{m-1}^a + F_{m+1}^a) \right] - \frac{1}{2i} \Delta_Z^* [u_2^{m-1} - u_2^{m+1}] [1 + F_m^a] + \frac{1}{2} \Delta_D^* [u_2^{m-2}(1 + F_{m-1}^a) + u_2^{m+2}(1 + F_{m+1}^a)] \\ & + \frac{1}{2i} \Delta_R^* u_3^m [F_{m-1}^a - F_{m+1}^a] + \frac{1}{2} \Delta_Z^* [u_3^{m-1} + u_3^{m+1}] [1 + F_m^a] + \frac{1}{2i} \Delta_D^* [u_3^{m-2}(1 + F_{m-1}^a) - u_3^{m+2}(1 + F_{m+1}^a)], \end{aligned} \quad (12a)$$

$$\frac{\partial u_2^m}{\partial t} = \Delta_R^* u_1^m [1 + F_m^a] + \frac{1}{2i} \Delta_Z^* [u_1^{m-1}(1 + F_{m-1}^a) - u_1^{m+1}(1 + F_{m+1}^a)] - \frac{1}{2} \Delta_D^* [u_1^{m-2}(1 + F_{m-2}^a) + u_1^{m+2}(1 + F_{m+2}^a)], \quad (12b)$$

$$\frac{\partial u_3^m}{\partial t} = -\frac{1}{2} \Delta_Z^* [u_1^{m-1}(1 + F_{m-1}^a) + u_1^{m+1}(1 + F_{m+1}^a)] - \frac{1}{2i} \Delta_D^* [u_1^{m-2}(1 + F_{m-2}^a) - u_1^{m+2}(1 + F_{m+2}^a)]. \quad (12c)$$

Solution of Eqs. (12a-12c) is the main subject of this paper. An analytic solution is possible in special cases, when only one of the three coupling–Rashba, Dresselhaus, and Zeeman—is present.¹⁸ If both types of SOC are absent, the problem reduces to the well-studied case of a partially spin-polarized FL, which supports the Silin-Leggett collective mode.^{10,11,19,20} If the magnetic field is absent and only type of SOC is present, the system (12a-12c) is also exactly soluble. This is the case of spin-chiral modes—collective oscillations of magnetization in the absence of magnetic field—which have recently been studied in Refs. 15, 16, 21–23. In all other cases, Eqs. (12a-12c) do not allow for an analytic solution. A numerical solution is, of course, possible, and will be discussed below. However, an important insight into the nature of solutions is gained by noticing that the original problem can be mapped onto an effective lattice model.

III. Quantum kinetic equation as an effective lattice model

Inspecting Eqs. (12a-12c), we notice that they are similar to the Schroedinger equations for the tight-binding model on a 1D lattice. In this analogy, the angular momentum (m) plays the role of the lattice site index, while $u_{1,2,3}^m$ can be viewed as orbitals located on site m , with three orbitals per site. Furthermore, the Rashba terms (those proportional to Δ_R^*) are “local”, in a sense that the time derivative of the orbital on site m is proportional to another orbital on the same site. Therefore, the Rashba terms play the role of on-site energies. On the other hand, the Zeeman terms (those proportional to Δ_Z^*) connect the time derivative of the orbital on site m to those on sites $m \pm 1$. One can then view those terms as generating “hopping” between the nearest neighbors. In the same way, the Dresselhaus terms (those proportional to Δ_D^*) generate hopping between next-to-nearest neighbors. It will be shown in more detail in Sec. V A

that, in the absence of the FL interaction ($F_n^a = 0$ for $\forall n$), the system is mapped onto a standard 1D tight-binding model with a single band, which corresponds to the continuum of spin-flip particle-hole excitations. The width of the band is determined by the combinations of the three energy scales: Δ_R , Δ_D , and Δ_Z .

Furthermore, harmonics of the Landau function, F_m^a , enter system (12a-12c) in two ways: some of them affect the Rashba terms, responsible for on-site energy shifts, while others affect the Zeeman and Dresselhaus terms, responsible for nearest- and next-to-nearest neighbors, correspondingly. The effect of F_m^a is *local*, i.e., harmonic F_m^a affects sites $m, m \pm 1$, and $m \pm 2$. Here comes another step in mapping: in the effective lattice language, the FL interaction is equivalent to “impurities”, which affect both on-site energies and bonds between adjacent sites.

Impurities on 1D lattice produce bound states with energies outside the band. In the original FL language, these bound states are nothing but the collective modes lying necessarily outside the continuum of particle-hole excitations. Therefore, studying a much simpler problem of bound states in the 1D tight-binding model, one can understand a much more complicated case of a FL with SOC and in the presence of the magnetic field.

The harmonic content of $F^a(\theta)$ determines how many sites (and bonds) are affected. For example, in the s -wave approximation, when $F^a(\theta) = \text{const}$ and therefore $F_m^a = \delta_{m,0} F_0^a$, only a small number of central sites (around $m = 0$) contain impurities. In the opposite case of a sharply peaked Landau function, i.e., when $F^a(\theta) = \text{const} \times \delta(\theta)$ and F_m^a does not depend on m , all impurities are identical and occupy all the sites. In this case, impurities are alloyed with the original lattice, and the bands of single-particle excitations and of collective modes merge into a new band of such an alloy. A more realistic Landau function monotonically decreases with θ , and thus F_m^a decrease with m as well. In the lattice language, this is equivalent to a *non-uniform ordered alloy*, in which stronger impurities occupy the central region of the lattice, and vice versa.

The key elements of mapping between the two models are summarized in Table I. We found it less instructive to present the details of mapping in the most general case, when all the three couplings–Rashba, Dresselhaus, and Zeeman–are present. Instead, we will work out these details for a number of subcases below.

IV. Effective lattice model with Rashba coupling only

To begin with, we consider the case without the magnetic field and Dresselhaus SOC. Although this case allows for an exact solution,¹⁵ it is still beneficial to understand it in the effective lattice model. With $\Delta_Z^* = \Delta_D^* = 0$, Eqs. (12a-12c) are reduced to

$$\partial_t u_1^m = -\gamma_1^m \frac{\Delta_R^*}{2} u_2^m; \quad \partial_t u_2^m = \gamma_2^m \frac{\Delta_R^*}{2} u_1^m; \quad \partial_t u_3^m = 0, \quad (13)$$

where $\gamma_1^m = 2 + F_{m+1}^a + F_{m-1}^a$ and $\gamma_2^m = 2(1 + F_m^a)$. In the absence of Zeeman and Dresselhaus terms, there is no hopping between sites of the effective lattice: the time evolution of $u_{1,2}^m$ is determined by $u_{2,1}^m$ on the same site. In this case, one can think of vector \mathbf{u}^m as of a classical spin on site m . Spins do not interact with each other but are subject to a spin-orbit “magnetic field”, directed along the x_3 axis and of magnitude $\Delta_R^*/2$. The effective Landé factor of these spins is anisotropic in the (x_1, x_2) plane with components γ_1^m and γ_2^m given above. The lattice is also *non-uniform* because γ_1^m and γ_2^m depend on the lattice site. Both anisotropy and site-dependence of the g -factor arise from the FL interaction. With $u_3^m = \text{const}$, the spins precess around the spin-orbit field, see Fig. 2a. A spin on site m precesses with frequency

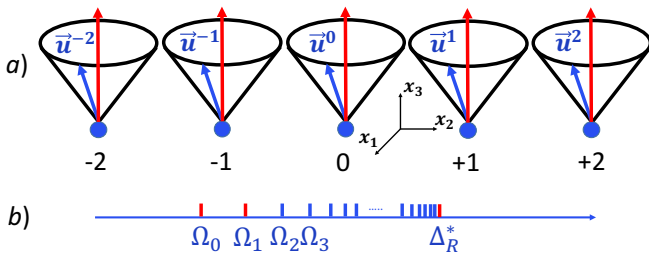


FIG. 2. a) Effective lattice model for collective modes in a Fermi liquid with Rashba spin-orbit coupling. Lattice sites $0, \pm 1, \pm 2 \dots$ correspond to the angular momenta parametrizing the non-equilibrium part of the occupation number, \mathbf{u} [Eq. (8)]. Each vector \mathbf{u}_m represents a classical spin coupled to an effective spin-orbit magnetic field (vertical red arrows) via an anisotropic and site-dependent Landé factor. Spins precess independently of each other with site-dependent frequencies, which are the frequencies of the collective modes [Eq. (14)]. b) The spectrum of the system consists of an infinite number of discrete levels, converging towards the continuum at Δ_R^* .

$$\Omega_m = \Delta_R^* \sqrt{\left[1 + \frac{1}{2}(F_{m+1}^a + F_{m-1}^a)\right] (1 + F_m^a)}. \quad (14)$$

These are the frequencies of the collective modes–chiral spin resonances.¹⁵ The continuum of particle-hole excitation in the Rashba-only case is represented by a single frequency $\Omega = \Delta_R^*$.²⁴ For any realistic interaction, the harmonics of $F^a(\theta)$ decrease with m ; also, for repulsive fermion-fermion interaction, $F_m^a < 0$ and thus $\Omega_m \leq \Delta_R^*$. Hence the discrete spectrum of the collective modes converges to the point of continuum, Δ_R^* , from below, see Fig. 2b.

Macroscopic magnetization is related to $\mathbf{u}(\theta_{\mathbf{p}})$ via

$$\mathbf{M} = \frac{g\mu_B}{4} \nu_F \text{Tr} \int_{\theta} \hat{\sigma}(\mathbf{u} \cdot \hat{\tau}), \quad (15)$$

As is obvious from the form of the τ -matrices [Eq. (7)], \mathbf{M} contains only the $m = 0$ and $m = \pm 1$ harmonics of \mathbf{u} . In other words, external magnetic and electric fields, which one applies to excite the collective modes, couple only to the effective classical spins on sites $m = 0, \pm 1$. These spins precess with frequencies

$$\Omega_0 = \Delta_R^* \sqrt{(1 + F_1^a)(1 + F_0^a)} \quad (16)$$

and

$$\Omega_1 = \Omega_{-1} = \Delta_R^* \sqrt{\left[1 + \frac{1}{2}(F_0^a + F_2^a)\right] (1 + F_1^a)}. \quad (17)$$

These are the frequencies that one expects to observe by ESR in zero magnetic field.

V. Partially-polarized Fermi liquid with Rashba spin-orbit coupling

A. Non-interacting case

Hopping between the sites of the effective lattice arises if at least two out of three couplings are present. To understand the effect of hopping, we first consider the non-interacting case, when $F^a(\theta) = 0$. To simplify the problem even further, we eliminate Dresselhaus SOC at first and restore it at the end of this section. With these simplifications, Eqs. (12a-12b) are reduced to

$$\begin{aligned} \partial_t u_1^m &= -\Delta_R u_2^m - \Delta_Z \left(\frac{u_2^{m-1} - u_2^{m+1}}{2i} - \frac{u_3^{m-1} + u_3^{m+1}}{2} \right), \\ \partial_t u_2^m &= \Delta_R u_1^m + \frac{1}{2i} \Delta_Z (u_1^{m-1} - u_1^{m+1}), \\ \partial_t u_3^m &= -\frac{1}{2} \Delta_Z (u_1^{m-1} + u_1^{m+1}). \end{aligned} \quad (18)$$

One can interpret these equations as an effective tight-binding model with three orbitals, $u_{1,2,3}^m$, on each lattice

TABLE I. Mapping of the Fermi-liquid theory onto an effective 1D tight-binding model.

Fermi-liquid kinetic equation	1D tight-binding model
angular momentum m	lattice site m
azimuthal angle of momentum \mathbf{p} , $\theta_{\mathbf{p}}$	lattice momentum
harmonic m of the components of distribution function $u_{1\dots 3}^m$	orbital wavefunctions on site m
Rashba spin-orbit coupling	on-site energy
Zeeman splitting	nearest-neighbor hopping
Dresselhaus spin-orbit coupling	next-to-nearest neighbor hopping
continuum of spin-flip particle-hole excitations	conduction band
collective modes	bound states

site, see Fig. 3a. The Rashba spin-orbit field (shown by vertical red arrows) couples to the u_1 and u_2 orbitals but not to u_3 . The Zeeman term gives rise to *orbital-selective* hopping between the nearest neighbors; allowed hoppings are indicated by orange arrows. For example, orbital u_1 is coupled to the orbitals u_2 and u_3 , but there is no hopping between the orbitals u_2 and u_3 .

The tight-binding picture is simplified considerably by eliminating orbitals u_2^m and u_3^m in favor of u_1^m . The time Fourier transform of the latter satisfies a much simpler equation

$$\Omega^2 u_1^m = (\Delta_R^2 + \Delta_Z^2) u_1^m + i\Delta_R \Delta_Z (u_1^{m+1} - u_1^{m-1}). \quad (19)$$

Equation (19) is reduced to standard form by introducing a new variable (“Bloch wavefunction”)

$$\psi_m \equiv i^{-m} u_1^m, \quad (20)$$

which satisfies²⁵

$$\Omega^2 \psi_m = (\Delta_R^2 + \Delta_Z^2) \psi_m - \Delta_R \Delta_Z (\psi_{m+1} + \psi_{m-1}). \quad (21)$$

The equation for the Bloch wavefunction contains only terms describing on-site energy [the first term on the right-hand side of Eq. (19)] and nearest-neighbor hopping [the second term]; all other terms cancel out. The eigenfrequency of Eq. (19)

$$\Omega(\theta_{\mathbf{p}}) = [\Delta_R^2 + \Delta_Z^2 - 2\Delta_R \Delta_Z \cos \theta_{\mathbf{p}}]^{1/2} \quad (22)$$

disperses with conjugate to m variable $\theta_{\mathbf{p}} \in (0, 2\pi)$, which plays the role of “lattice momentum”. At the same time, $\theta_{\mathbf{p}}$ is nothing else but the azimuthal angle of \mathbf{p} , so we worked our way back to original system (11a-11c), which can now be viewed as written in the “momentum representation”.

The minimum and maximum values of $\Omega(\theta_{\mathbf{p}})$ mark the edges of the “band”, which corresponds to the continuum of spin-flip excitations (shaded rectangular in Fig. 3b). The bandwidth is given by

$$\Omega_c = |\Delta_R| + \Delta_Z - ||\Delta_R| - \Delta_Z|. \quad (23)$$

Likewise, with both SOC present but in the absence of the magnetic field, the band occupies an interval from $||\Delta_R| - |\Delta_D||$ to $|\Delta_R| + |\Delta_D|$.

Of course, one can get the same results in the momentum representation, i.e., directly from Eqs. (11a-11c). Setting $F^a(\theta) = 0$ and $\Delta_D = 0$ in these equations, we obtain

$$\begin{aligned} \partial_t u_1(\theta_{\mathbf{p}}) &= -(\Delta_R + \Delta_Z \sin \theta_{\mathbf{p}}) u_2(\theta_{\mathbf{p}}) + \Delta_Z \cos \theta_{\mathbf{p}} u_3(\theta_{\mathbf{p}}), \\ \partial_t u_2(\theta_{\mathbf{p}}) &= (\Delta_R + \Delta_Z \sin \theta_{\mathbf{p}}) u_1(\theta_{\mathbf{p}}), \\ \partial_t u_3(\theta_{\mathbf{p}}) &= -\Delta_Z \cos \theta_{\mathbf{p}} u_1(\theta_{\mathbf{p}}). \end{aligned} \quad (24)$$

Eliminating u_2 and u_3 from equations above, one obtains a second-order equation for u_1 which is an equivalent of Eq. (19) in the momentum space. [The only difference between the two results is a $\pi/2$ shift of $\theta_{\mathbf{p}}$ which is effected by transformation (20).]

The physical reason for the continuum to have a finite width is anisotropy of the electron spectrum in the presence of at least two couplings. At $q = 0$, particle-hole excitations corresponds to vertical transitions between spin-split subbands with frequencies

$$\Omega_c = |\varepsilon_+ - \varepsilon_-|, \quad (25)$$

where

$$\begin{aligned} \varepsilon_{\pm} &= \frac{p^2}{2m_b} \pm \left[(\alpha^2 + \beta^2) p^2 + \frac{\Delta_Z^2}{4} \right. \\ &\quad \left. + (\alpha + \beta) p_2 \Delta_Z - 2\alpha\beta (p_1^2 - p_2^2) \right]^{1/2} \end{aligned} \quad (26)$$

are the eigenenergies of Hamiltonian (1). As \mathbf{p} wraps around the FS, the eigenenergies vary between the minimum and maximum values. This variation determines the width of the continuum. Setting $\beta = 0$ and $p = p_F$ in Eq. (26), we see that Eq. (25) gives the same result as Eq. (22).

Restoring Dresselhaus SOC in the equations of motion does not lead to qualitative changes. With all the three couplings present, Eq. (22) for the eigenfrequency is replaced by

$$\begin{aligned} \Omega(\theta_{\mathbf{p}}) &= [\Delta_R^2 + \Delta_D^2 + \Delta_Z^2 + 2(\Delta_R + \Delta_D)\Delta_Z \sin \theta_{\mathbf{p}} \\ &\quad - 2\Delta_R \Delta_D \cos 2\theta_{\mathbf{p}}]^{1/2}. \end{aligned} \quad (27)$$

As before, the maximum and minimum values of $\Omega(\theta_{\mathbf{p}})$ determine the bandwidth, but its explicit form is now more complicated and we refrain from presenting it.

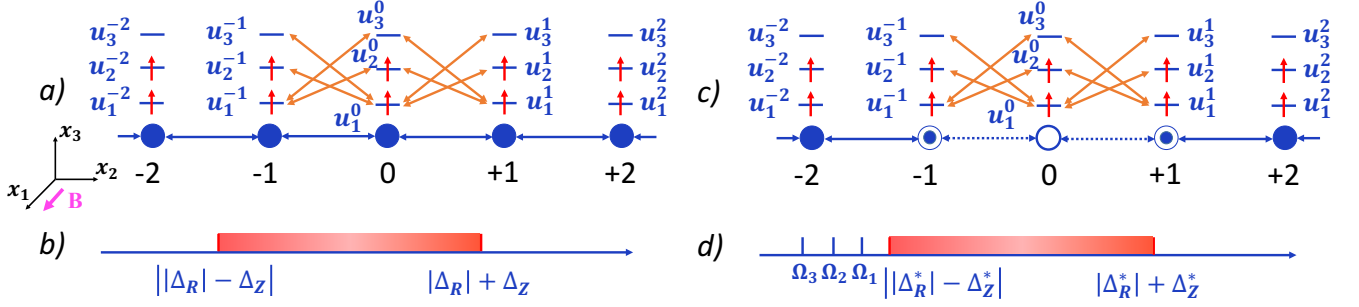


FIG. 3. a) Effective lattice model for a non-interacting electron gas with Rashba spin-orbit coupling and in the presence of an in-plane magnetic field (B). As in Fig. 2, lattice sites $0, \pm 1, \pm 2 \dots$ correspond to the angular momenta parametrizing the non-equilibrium part of the occupation number, \mathbf{u} [Eq. (8)] but now components $u_{1\dots 3}^m$ play the role of on-site orbitals. The spin-orbit field (red vertical arrows) is coupled to orbitals u_1^m and u_2^m , while B leads to nearest-neighbor hopping with orbital-selective matrix elements. Allowed hoppings between sites $-1, 0$, and $+1$ are indicated by orange arrows, and similar for other sites. b) The spectrum consists of a finite-width band (shaded rectangular), which corresponds to the continuum of spin-flip particle-hole excitations. c) Same as in a) but for the FL case. The FL interaction, parametrized by the harmonics of the Landau function, F_m^a , has an effect of *bond disorder*, which modifies the hopping matrix elements. If F^a has only the $m = 0$ harmonic, the "impurity" (open circle) is located on the $m = 0$ site, as shown in the figure; higher harmonic of F^a affect other sites. d) The spectrum consists of the continuum (shaded) and discrete bound states, which are the collective modes of the FL.

In the special case when two out of the three couplings are absent, the spectrum becomes isotropic and the continuum shrinks to a single point. This case was discussed in Sec. IV.

B. Interacting case

We now discuss a FL with Rashba SOC in the presence of magnetic field. This case is described by Eqs. (12a-

12b) with $\Delta_D^* = 0$. The FL interaction renormalizes both on-site energies and hopping matrix elements, and its effect is analogous to that of "impurities" which introduce both on-site and bond disorder. The m^{th} harmonic of F^a affects energies on sites m and $m \pm 1$ and bonds between these sites. In the case of s -wave interaction ($F_m^a = F_0^a \delta_{m0}$), for example, we have impurities on sites 0 and ± 1 , and the bonds between sites 0 and ± 1 are "defective", see Fig. 3c.

Eliminating again u_2^m and u_3^m in favor of u_1^m , we obtain an equation for the time Fourier transform of the Bloch wavefunction ψ_m defined by Eq. (20):

$$\Omega^2 \psi_m = \left[\Delta_R^{*2} (1 + F_m^a) \left(1 + \frac{F_{m+1}^a + F_{m-1}^a}{2} \right) + \Delta_Z^{*2} (1 + F_m^a)^2 \right] \psi_m - \Delta_R^* \Delta_Z^* \left[\left(1 + \frac{F_m^a + F_{m+1}^a}{2} \right) (1 + F_{m+1}^a) \psi_{m+1} + \left(1 + \frac{F_{m-1}^a + F_m^a}{2} \right) (1 + F_{m-1}^a) \psi_{m-1} \right], \quad (28)$$

Both the on-site and hopping terms are renormalized by the FL interaction. The equation above is the key one from which all the limiting cases can be derived, which is what we will be doing in the rest of this section. Before going into particular models for F_m^a though, we make one general observation. An attractive impurity on a 1D lattice has at least one bound state below the band, while a repulsive one has at least one bound state above the band. (One can think of these states as donor and acceptor levels in a semiconductor). If all $F_m^a < 0$, the on-site energies in Eq. (28) are reduced compared to the non-interacting case [cf. Eq. (21)]. This case corresponds to attractive impurities, with bound states

(collective modes) below the band (continuum); it is vice versa for $F_m^a > 0$, when the impurities are repulsive and the bound states are above the band. On the other hand, the number of bound states and their relative spacings will be specific for particular models, which we are now going to study.

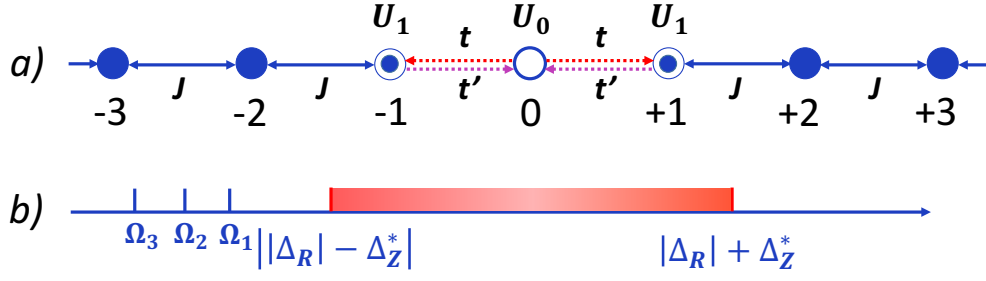


FIG. 4. a) Effective lattice model for two dimensional FL with s -wave approximation for the Landau function in the presence of Rashba spin-orbit coupling and in-plane magnetic field (B). For the simplest interaction (s -wave), lattice sites $m = 0$ and ± 1 are disordered. In the single-orbital basis, ψ_i , the on-site energies at sites $m = \pm 1$ (dotted pink arrow) are different from that at site $m = 0$ (dotted brown arrow), [Eq.(29)]. Furthermore, all the other sites which form a continuum also have different on-site energies from disordered sites (solid red arrow). The bond disorder is *chiral*: the amplitude of hopping from $m = 0$ to $m = \pm 1$ (dotted orange arrows) is not the same as from $m = \pm 1$ to $m = 0$ (dotted green arrows). b) The spectrum consists of the continuum (shaded) and discrete bound states, which are the collective modes of the FL.

C. s -wave approximation for the Landau function to

1. Exact solution of the equations of motion.

The first case is the s -wave approximation for the Landau function, when $F_m^a = \delta_{m,0} F_0^a$ and Eq. (28) is reduced

$$\begin{aligned} \Omega^2 \psi_m = & (\Delta_R^2 + \Delta_Z^{*2}) \psi_m + \delta_{m,0} F_0^a [\Delta_R^2 + \Delta_Z^{*2} (2 + F_0^a)] \psi_m + (\delta_{m,1} + \delta_{m,-1}) \frac{F_0^a}{2} \Delta_R^2 \psi_m \\ & - \Delta_R \Delta_Z^* \left\{ \psi_{m+1} + \psi_{m-1} + \delta_{m,0} \frac{F_0^a}{2} (\psi_1 + \psi_{-1}) + (\delta_{m,1} + \delta_{m,-1}) \frac{F_0^a}{2} (3 + F_0^a) \psi_0 \right\}. \end{aligned} \quad (29)$$

We re-arranged the equation above in such a way that the first line of its right-hand side correspond to on-site energies while the second line correspond to hopping. [According to Eq. (6), Δ_R is not renormalized in the s -wave approximation.] The first term in the first line describes on-site energies of undistorted lattice, the other two terms account for energy shifts due to impurities at $m = 0$ and $m = \pm 1$. Next, the first term in the curly brackets describes hopping via regular bonds, while the other two terms describe hopping via defect bonds connecting the $m = 0$ and $m = \pm 1$ sites. Notice that bond disorder is *chiral*: the amplitude of hopping from $m = 0$ to $m = \pm 1$ is not the same as from $m = \pm 1$ to $m = 0$, as indicated in Fig. 4. This means that the effective Hamiltonian corresponding to the equations of motion (29) is non-Hermitian: bond disorder is described by a non-Hermitian term $J\Psi_0^\dagger \Psi_{\pm 1} + J'\Psi_{\pm 1}^\dagger \Psi_0$ with $J \neq J'$. Non-Hermiticity arises from broken time-reversal symmetry in our original problem. It does not present any difficulties, however, because the eigenvalues of Eq. (29) are real.

Equation (29) can be solved by a slight modification of the standard method for finding the bound states on 1D lattices.²⁶ Namely, we choose wavefunctions ψ_0 and $\psi_{\pm 1}$ as independent variables. Starting from sites $m = \pm 2$, we assume that the wavefunction of the bound state decreases exponentially with m , i.e.,

$$\psi_{\pm(|m|+2)} = e^{-(|m|+1)\lambda} \psi_{\pm 1} \quad (30)$$

with $\text{Re}\lambda > 0$. Applying this Ansatz to any three nearest neighbors of undistorted lattice, we obtain a relation between Ω^2 and λ

$$\Omega^2 = \Delta_R^2 + \Delta_Z^{*2} - 2\Delta_R \Delta_Z^* \cosh \lambda \quad (31)$$

or

$$e^{-\lambda} = \frac{(1 + x^2 - y^2) \pm \sqrt{(1 + x^2 - y^2)^2 - 4x^2}}{2x}, \quad (32)$$

where $y = \Omega/\Delta_R$ and $x = \Delta_Z^*/\Delta_R$. (To simplify the analysis, we will assume that $\Delta_R > 0$.) Substituting $m = 0, \pm 1$ into Eq. (29) and using Ansatz (30) to exclude $\psi_{\pm 2}$, we obtain a closed system for ψ_0 and $\psi_{\pm 1}$

$$\begin{bmatrix} 1 + x^2 - y^2 + \frac{1}{2}F_0^a - xe^{-\lambda} & -x[1 + \frac{1}{2}F_0^a(3 + F_0^a)] & 0 \\ -x(1 + \frac{1}{2}F_0^a) & 1 + x^2 - y^2 + F_0^a[1 + (2 + F_0^a)x^2] & -x(1 + \frac{1}{2}F_0^a) \\ 0 & -x[1 + \frac{1}{2}F_0^a(3 + F_0^a)] & 1 + x^2 - y^2 + \frac{1}{2}F_0^a - xe^{-\lambda} \end{bmatrix} \begin{bmatrix} \psi_{-1} \\ \psi_0 \\ \psi_1 \end{bmatrix} = 0. \quad (33)$$

Equating the determinant of this system to zero and using Eq. (32), we obtain a transcendental equation for eigenfrequencies. This equation happens to have an analytic solution, but its explicit form is quite lengthy, and we delegate it to Appendix B, focusing here on Fig. 5 obtained by plotting the results in Eq. (B1) of that Appendix.

At a special value of the magnetic field, when $\Delta_Z^* = \Delta_R$, the gap in the continuum closes. To the left of this point, i.e., for $\Delta_Z^* < \Delta_R$, there are up to three collective modes which, at $\Delta_Z^* = 0$ coincide with spin-chiral modes, considered in Sec. IV. The frequencies of these modes at $\Delta_Z^* = 0$ are given by Eqs. (16) and (17) with $F_1^a = F_2^a = 0$. A finite magnetic field lifts the degeneracy of the $m = \pm 1$ modes which now disperse with Δ_Z^* , as shown in Fig. 5, left. At some critical values of the field, these modes run into the continuum, while the $m = 0$ mode disperses down until the closing point of the gap. To the right of this point, i.e., for $\Delta_Z^* > \Delta_R$, there is only one mode which, for $\Delta_Z^* \gg \Delta_R$, transforms into the Silin-Leggett mode with frequency equal to the bare Larmor frequency, Ω_L , see Fig. 5, right. The results described above are in exact correspondence to those found within RPA for the spin susceptibility of a partially polarized FL with Rashba SOC.⁹

2. Physical interpretation within the effective lattice model

The spectrum of the collective modes shown in Fig. 5 has several distinct features, namely: i) two higher-energy modes in the region $\Delta_Z^*/\Delta_R < 1$ disappear at certain values of the magnetic field; ii) the lowest-energy mode runs into the continuum at $\Delta_Z^*/\Delta_R = 1$; and iii) there is only one mode for $\Delta_Z^*/\Delta_R > 1$. In this section, we show that all these features can be understood within the effective lattice model as a result of competition between the on-site impurities and hopping, both between normal and impurity sites.

The effective tight-binding model corresponding to Eq. (29) is shown in Fig. 4a. This equation is an eigenvalue problem for the *square* of the frequency, and its right-hand side contains the squares of the various energy scales. To make an analogy with the tight-binding model complete, we will be referring to quantities with units of $[\text{energy}]^2$ simply to as “energies”. In this way, Ω^2 becomes the energy of the bound state E and hopping energy between normal sites is

$$J = \Delta_R \Delta_Z^*. \quad (34)$$

The potential energies on the impurity sites will be measured relative to the on-site energy of undistorted lattice,

$\Delta_R^2 + \Delta_Z^{*2}$. Then the potential energy of the impurities at sites $m = 0$ and $m = \pm 1$ are given by

$$\begin{aligned} U_0 &= F_0^a \Delta_R^2 + F_0^a (2 + F_0^a) \Delta_Z^{*2}, \\ U_1 &= (F_0^a/2) \Delta_R^2, \end{aligned} \quad (35)$$

correspondingly. Finally, the hopping amplitudes between sites $m = 0$ and $m = \pm 1$ are

$$\begin{aligned} t &= \left(1 + \frac{F_0^a}{2}\right) \Delta_R \Delta_Z^*, \text{ for } 0 \rightarrow \pm 1; \\ t' &= \left[1 + \frac{F_0^a}{2}(3 + F_0^a)\right] \Delta_R \Delta_Z^*, \text{ for } \pm 1 \rightarrow 0. \end{aligned} \quad (36)$$

For $F_0^a < 0$, the impurities are *attractive*, i.e., $U_0, U_1 < 0$, and the defective bonds are *weaker* than the normal ones, i.e., $t, t' < J$.

a. Three attractive impurities.

Although to explain every detail of the spectrum in Fig. 5, we will need to take into account all of the elements listed above, one the features—the disappearance of two higher-energy modes—can be understood qualitatively by ignoring bond defects, i.e., setting $t = t' = J$. Then we have a tight-binding model with normal bonds between all sites and with three impurities, see Fig. 6a. It is also convenient to measure all energies in units of J , i.e., to set $J = 1$.

For an even simple case of one impurity, it is well-known that there always exists a bound state, located either below (for $U_0 < 0$) or above (for $U_0 > 0$) the conduction band. In the context of semiconductors, these states are known as donor and acceptor states, i.e., the bound states of electrons and holes, respectively. A tight-binding band has electron-like states below the inflection point and hole-like states above that point, so the donor and acceptor states occur also in this case. Since our impurities are attractive, we will focus on this case from now on.

Given that one impurity has one bound state, it is natural to expect that three impurities will have up to three bound states. In the continuum limit, this corresponds to a 1D potential well of finite width a and depth U_0 , which has at least one bound state but may have two, three, etc. states, if the product $-U_0 a$ exceeds some critical values. In the lattice case, we use Ansatz (30) to write down a closed system of equations for the three impurity sites

$$\begin{aligned} E\psi_0 &= U_0\psi_0 - \psi_1 - \psi_{-1}, \\ E\psi_{\pm 1} &= U_1\psi_{\pm 1} - \psi_0 - \psi_{\pm 1}e^{-\lambda}, \end{aligned} \quad (37)$$

complemented by the relation between E and λ , which must be satisfied for any three normal sites: $E =$

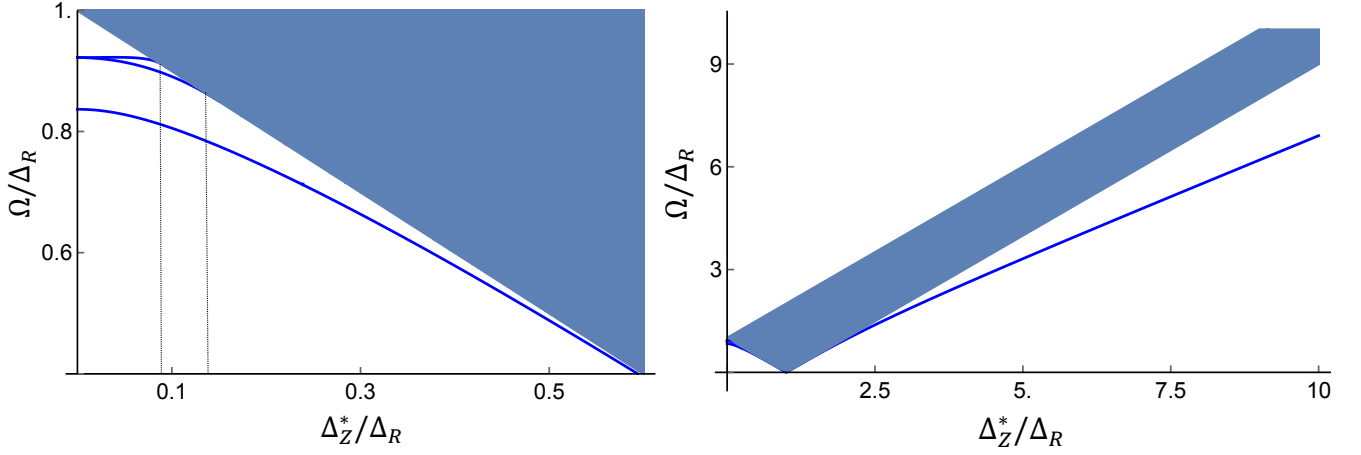


FIG. 5. Collective modes of a FL with Rashba SOC and in the presence of an in-plane magnetic field. The Landau function is taken in the s -wave approximation: $F^a(\theta) = F_0^a = -0.3$. Δ_Z^* is the (renormalized) Zeeman energy and Δ_R is the Rashba energy splitting. Left: $\Delta_Z^* \leq \Delta_R$. Right: $\Delta_Z^* > \Delta_R$.

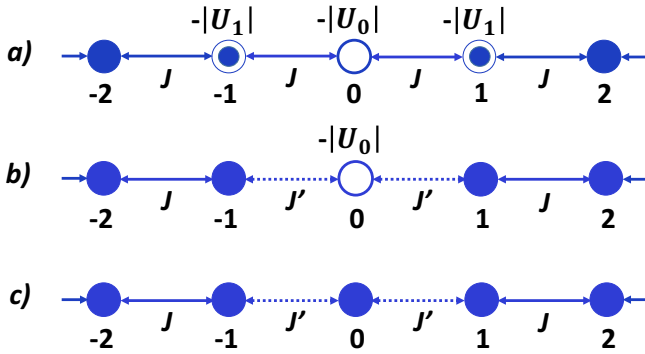


FIG. 6. One-dimensional tight-binding models. a) Three on-site attractive impurities at site $m = 0$ and $m = \pm 1$. b) One attractive impurity at $m = 0$ and two defective bonds between sites $m = 0$ and $m = \pm 1$ with hopping amplitudes J' . c) Two defective bonds between sites $m = 0$ and $m = \pm 1$ with hopping amplitudes J' . The hopping amplitude for normal bonds, J , is set to unity.

$-2 \cosh \lambda$. For even-parity solutions, $\psi_1 = \psi_{-1}$. Substituting this into Eq. (37), we obtain an equation for corresponding eigenenergies $(E - U_1 + e^{-\lambda})(E + U_0) = 2$. For odd-parity solutions, $\psi_1 = -\psi_{-1}$ and hence $\psi_0 = 0$. This immediately gives $E - U_1 + e^{-\lambda} = 0$. In Appendix ??, we show that there are up to two even-parity bound states (one of them is the lowest-energy state which is always present) and up to one odd-parity bound states. The phase diagram of the three-impurity model is shown in Fig. 7.

Our original problem corresponds to a tight-binding model with parameters given by Eqs. (34), (35), and (36). We notice that in the limit of $\Delta_Z^* \ll \Delta_R$, the potential energies on all three impurity sites are on the order of Δ_R^2 , which is much larger than the bandwidth $2J = 2\Delta_R\Delta_Z^*$. Thus we have three strong impurities with

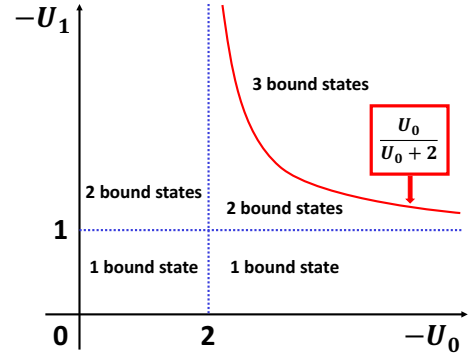


FIG. 7. Phase diagram for bound states in a one-dimensional tight-binding model with three attractive on-site impurities, as shown in Fig. 6a.

the maximum number of bound states, which is three. As Δ_Z^* is increased, the bandwidth increases as Δ_Z^* but the potential energies increase only as Δ_Z^{*2} . Therefore, impurities get weaker and we loose first the highest and then next-to-highest-energy bound state, when the ratio of the potential energy to the bandwidth decreases below some critical values. This explain the disappearance of the two out of three collective modes at certain values of $\Delta_Z^*/\Delta_R < 1$.

b. *Competition between on-site impurities and defective bonds.*

The three-impurity model is unable to explain an interesting feature of the spectrum in Fig. 5: the lowest energy collective mode approaches the continuum both from the left (panel a) and from the right (panel b) and touches the continuum at one particular point, where $\Delta_Z^* = \Delta_R$. This point corresponds to closing the gap in the continuum and, from the collective-mode point-of-view, this behavior seems natural. However, from the lattice point-of-view, it means that bound states disap-

pears for a certain choice of the parameters of the tight-binding model, which cannot happen if only on-site impurities are present. The explanation of this feature lies in the competition between on-site impurities and adjacent defective bonds, which we consider in this section.

To understand this competition qualitatively, we consider a toy model with one attractive impurity at $m = 0$ and two defective bonds (with tunneling amplitudes J'), see Fig. 6b. To analyze the role of the defective bonds, we consider a special case when there is no impurity but the bonds are defective. In this case, there is also a bound state but it occurs only if the defective bonds are *stronger* than the normal ones, i.e., $|J'| > J = 1$. (There are actually two bound states: one above and one below the conduction band.)

The difference between the cases of $|J'| > 1$ and $|J'| < 1$ can be understood by going to the continuum limit, where a local change in J leads to two effects: a bandwidth offset and a change in the effective mass. The latter does not give rise to a bound state by itself. Indeed, a solution of the Schrodinger equation with a step-like variation in the mass does not have an evanescent solution, which means that the bound state is impossible. On the other hand, a local variation in the bandwidth gives rise to a bound state, if the band is wider in the central region but not if it is narrower, see Fig. 8. (This

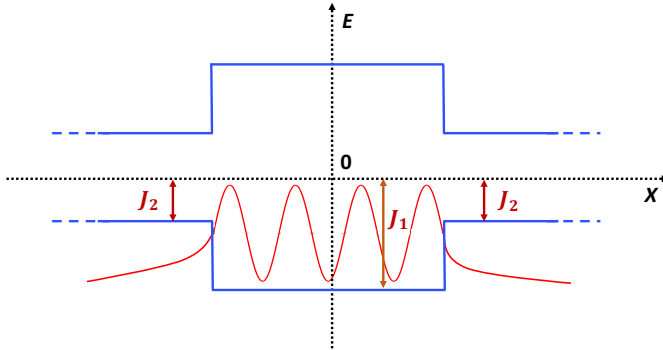


FIG. 8. A bound state in a junction between a wide-band and narrow-band materials. Electrons with energies $J_2 < |E| < J_1$ are confined to the central region.

effect is dual to formation of a bound state in a narrow-gap semiconductor sandwiched in between two wide-gap semiconductors.²⁷⁾

Suppose now that an attractive impurity at $m = 0$ is connected to the $m = \pm 1$ sites via weak bonds with $|J'| < 1$, as in Fig. 6b. Because no bound state exists in the presence of weak bonds only, there should be a competition between the impurity, which would like to have a bound state, and weak bonds, which do not. As the bonds get weaker, the bound state becomes shallower until, at some critical value of J' , it merges with the band. (As shown in Appendix A 3, this happens if $|U_0| \leq 2$ and at the critical bond strength of $|J_c| = \sqrt{1 - |U_0|/2}$.)

c. End points of the spectra.

Since the defective bonds in our case are indeed weak [see Eq. (36)], we now understand qualitatively the mechanism by which the lowest-energy collective mode runs into the continuum. However, it does not explain why this happens precisely at $\Delta_Z^* = \Delta_R$ rather than at some arbitrary value of Δ_Z^* . To understand this, we need to return to the full tight-binding model in Fig. 4a, which contains all elements of the original problem, i.e., three impurities, and two defective and chiral bonds with $t \neq t'$, with parameters exactly as in Eqs. (34), (35), and (36).

The 3×3 system for the most general model reads

$$\begin{aligned} E\psi_0 &= U_0\psi_0 - t(\psi_{-1} + \psi_1), \\ E\psi_{\pm 1} &= U_1\psi_{\pm 1} - t'\psi_0 - \psi_{\pm 1}e^{-\lambda}, \end{aligned} \quad (38)$$

again along with $E = -2\cosh \lambda$. Selecting even- and odd-parity solutions, we obtain equations for the their eigenvalues (here we restore J for clarity)

$$(E - U_1 + Je^{-\lambda})(E - U_0) = 2tt', \text{ even}; \quad (39a)$$

$$E - U_1 + Je^{-\lambda} = 0, \text{ odd}. \quad (39b)$$

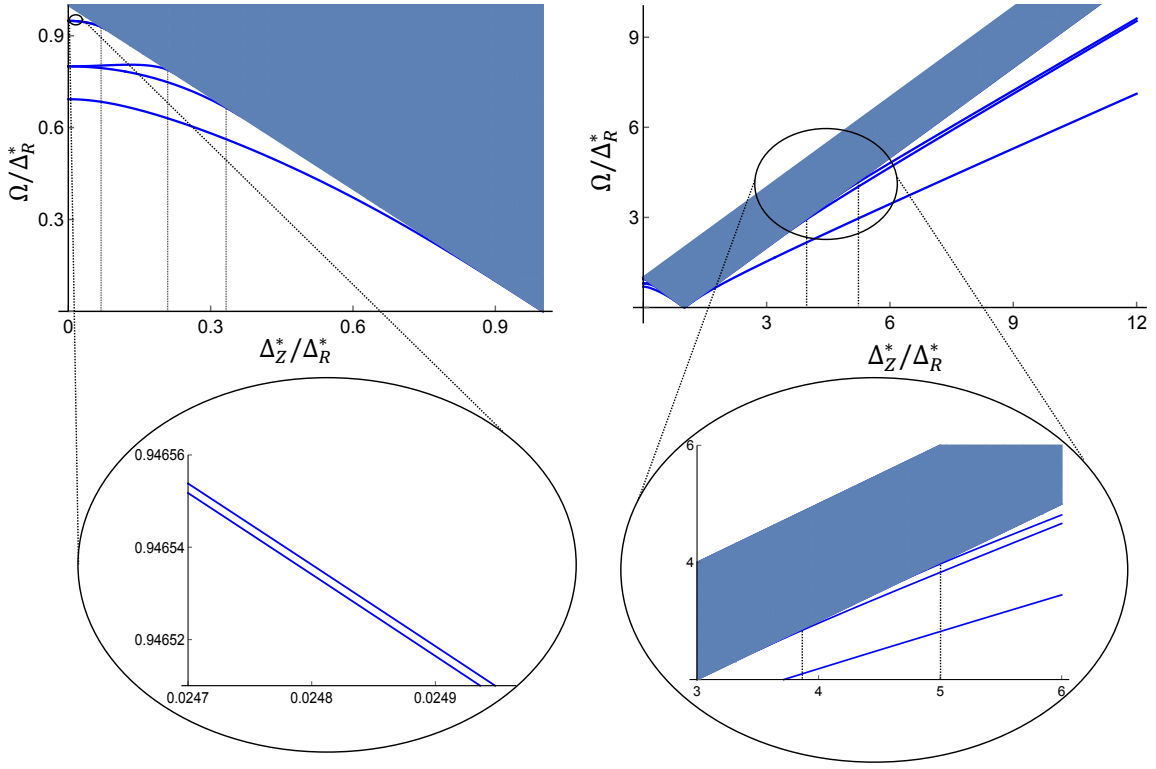
We know that the lowest collective mode corresponds to the even-parity bound state, therefore, the condition on its disappearance must follow from Eq. (39a). The bound states approaches the continuum when $E = -2J = -2\Delta_R\Delta_Z^*$. Substituting this value for the E the rest of the parameters from Eqs. (35) and (36) into Eq. (39a), we find that one of its two solutions is $\Delta_Z^* = \Delta_R$, which is indeed the gap-closing point. The second solution is $\Delta_Z^* = -F_0^a/[2(2 + F_0^a)]\Delta_R$. This is the point where the highest-energy collective mode, which is also of even parity, runs into the continuum (cf. Fig. 5a). Finally, substituting the same parameters into Eq. (39b), we find that the odd-parity collective mode runs into the continuum at $\Delta_Z^* = -F_0^a\Delta_R/2$. The analytic results for the three end points of the spectrum are in precise agreement with the exact solution in Appendix B.

d. Strong magnetic field: $\Delta_Z^* > \Delta_R$.

As Fig. 5 shows, there is only one bound state for $\Delta_Z^* > \Delta_R$. It is easier to understand this case starting from the limit of $\Delta_Z^* \rightarrow \infty$, where the Rashba term is negligibly small. In this limit, hopping disappears and we have decoupled sites with on-site energies Δ_Z^{*2} on all sites but $m = 0$, where the on-site energy is given by bare Zeeman splitting, Δ_Z^2 . This energy gives the frequency of the Silin-Leggett collective mode, while sites with $m \neq 0$ form a continuum at Δ_Z^* . It is intuitively obvious that small Δ_R cannot change the picture qualitatively: we will still have just one bound state with a renormalized frequency. Indeed, expanding the exact solution in Eq. (B1) for $\Delta_Z^* \gg |\Delta_R|/|F_0^a|$, we obtain

$$\Omega_L = \Delta_Z + \frac{(2 + 3F_0^a)(1 + F_0^a)}{4F_0^a} \frac{\Delta_R^2}{\Delta_Z} + \dots, \quad (40)$$

which coincides with the RPA result of Ref. 9 upon identifying the dimensionless coupling constant u with $-F_0^a$.



H

FIG. 9. Collective modes of a FL with Rashba SOC and in the presence of an in-plane magnetic field. The Landau function is taken in the $s + p$ approximation: $F^a(\theta) = F_0^a + 2F_1^a \cos \theta$. In the main panels, $F_0^a = -0.4$ and $F_1^a = -0.2$. The zooms show two almost degenerate higher energy modes for $F_0^a = -0.4$ and $F_1^a = -0.4$. The magnitude of F_1^a was increased to resolve the splitting.

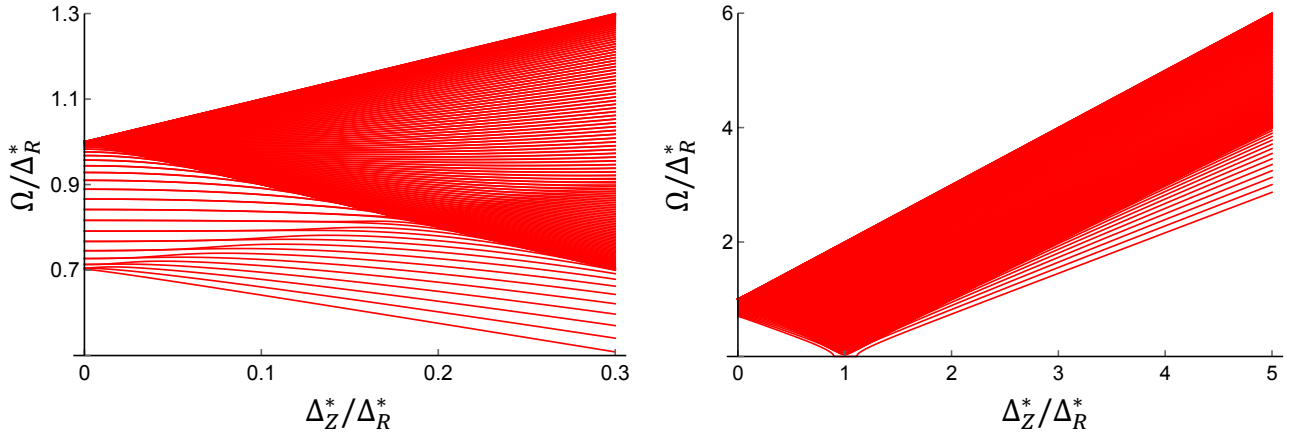


FIG. 10. Collective modes of a FL with Rashba SOC and in the presence of an in-plane magnetic field for a model form of the Landau function: $F_m^a = F_0^a \exp(-m^2/m_0^2)$ with $F_0^a = -0.3$ and $m_0 = 10$.

Notice that the Kohn theorem—independence of the Larmor frequency of the electron-electron interactions—holds for the leading term in Eq. (40) but is violated already for the first correction due to the presence of SOC.

As Δ_Z^* decreases, the impurity at $m = 0$ is still very strong (the ratio of its potential energy to the bandwidth is on the order of $\Delta_Z/\Delta_R \gg 1$), while the impurities at

$m \pm 1$ are weak (the corresponding ratio is on the order of $\Delta_R/\Delta_Z \ll 1$). In the case, we have only one bound state (cf. phase diagram in Fig. 7). As Δ_Z^* becomes comparable to Δ_R^* , the strengths of all the three impurities become comparable to each other and to the bandwidth, and more bound states may have appeared. However, our model is fine-tuned by the choice of parameters cor-

responding to the original FL kinetic equation, and with this choice there is only one bound state for $\Delta_Z^* > \Delta_R$, which touches the continuum at $\Delta_Z^* = \Delta_R$.

To conclude this section, we re-iterate that all the features of the collective mode spectrum are accounted for in the effective-lattice description.

D. Beyond s -wave approximation for the Landau function

In the previous section, we focused on the s -wave approximation for the Landau function. In this section, we analyze a more general case, beginning with the Landau function which has both $m = 0$ and $m = 1$ harmonics ($s + p$ -wave approximation). In the language of the effective-lattice model, this case corresponds to five impurities (on sites $m = 0, \pm 1, \pm 2$). The spectrum of the collective mode for this case is plotted in Fig. 9. Correspondingly, there are five spin-chiral resonances in zero magnetic field, which evolve into up to five collective modes as Δ_Z^* is increased up to Δ_R^* (the left panel). A zoom below the main panel emphasizes a small but finite splitting between the two high-energy modes. As the field increases, four out of five modes run into the continuum, following the same mechanism as for three impurities explained in Sec. VC 2 a. On the opposite side of the spectrum, for $\Delta_Z^* \rightarrow \infty$, we now have two Silin-Leggett modes. At finite but small ratio of Δ_R^*/Δ_Z^* , the higher-energy Silin-Leggett mode splits into two modes, both of which run into the continuum at some critical values of Δ_R^*/Δ_Z^* . The remaining low-energy mode grazes the continuum at touches is at gap-closing point. The same happens to the low-energy mode approaching the gap closing point from weak-field side.

If the Landau function contains all harmonics, one has to resort to numerical diagonalization of Eq. (28) for a particular form of the Landau function. We choose an artificial but reasonable model, in which $F_m^a = F_0^a e^{-m^2/m_0^2}$. Numerical results for $F_0^a = -0.3$ and $m_0 = 10$ are shown in Fig. 10. The spectrum is denser at lower energies because the first few harmonics of the Landau functions with $m < m_0$ are close to F_0^a , and their frequencies at $\Delta_Z = 0$ are given by Eq. (14): $\Omega_m \approx \Delta_R$. In the same approximation, the continuum is at $\Delta_R^* = \Delta_R(1 + F_1^a) \approx \Delta_R/(1 + F_0^a) > \Delta_R$. The modes with $m > m_0$ fill in the gap in between Δ_R and $\Delta_R^*/(1 + F_0)$. Although the collective mode spectrum is very dense, the mode remain discrete as long as m_0 is finite. In the effective-lattice language, we have an alloy with $\sim m_0$ of roughly comparable impurities occupying the central region. Both to the left and to the right from the central region, there are semi-infinite domains of weaker impurities whose strengths decrease rapidly away from the central region.

VI. A Fermi liquid with Rashba and Dresselhaus spin-orbit coupling

In this section, we consider the case when both Rashba and Dresselhaus SOC are present but there is no external magnetic field. This situation is similar to that of the magnetic field and Rashba SOC except for hopping is now of the next-to-nearest neighbor type. This will lead to important differences in the collective mode spectrum.

Setting Δ_Z^* Eqs. (12a -12c), reducing the system of equations to a single equation for u_1^m as before, and introducing a wavefunction via Eq. (20), we obtain the effective tight-binding model for this case

$$\begin{aligned} \Omega^2 \psi_m = & (\Delta_R^{*2} + \Delta_D^{*2})(1 + F_m^a) \left[1 + \frac{1}{2}(F_{m+1}^a + F_{m-1}^a) \right] \psi_m - \Delta_R^* \Delta_D^* (1 + F_{m-2}^a) (1 + F_{m-1}^a) \psi_{m-2} \\ & - \Delta_R^* \Delta_D^* (1 + F_{m+2}^a) (1 + F_{m+1}^a) \psi_{m+2}. \end{aligned} \quad (41)$$

The effective lattice is bipartite: every even (odd) site is coupled to the nearest even (odd) sites but there is no coupling between sites of different parity. It is convenient then to consider the lattice as being composed of two decoupled sublattices which contain only even

or only odd sites, with nearest-neighbor hopping within each sublattice. Introducing the sublattice wavefunctions as $\chi_l = \psi_{2l}$ and $\xi_l = \psi_{2l+1}$, we obtain two independent equations for each sublattice

$$\begin{aligned}
\Omega^2 \chi_l &= (\Delta_R^{*2} + \Delta_D^{*2})(1 + F_{2l}^a) \left[1 + \frac{1}{2}(F_{2l+1}^a + F_{2l-1}^a) \right] \chi_l - \Delta_R^* \Delta_D^* (1 + F_{2l-2}^a) (1 + F_{2l-1}^a) \chi_{l-1} \\
&\quad - \Delta_R^* \Delta_D^* (1 + F_{2l+2}^a) (1 + F_{2l+1}^a) \chi_{l+1}, \\
\Omega^2 \xi_l &= (\Delta_R^{*2} + \Delta_D^{*2})(1 + F_{2l+1}^a) \left[1 + \frac{1}{2}(F_{2l+2}^a + F_{2l}^a) \right] \xi_l - \Delta_R^* \Delta_D^* (1 + F_{2l-1}^a) (1 + F_{2l}^a) \xi_{l-1} \\
&\quad - \Delta_R^* \Delta_D^* (1 + F_{2l+3}^a) (1 + F_{2l+2}^a) \xi_{l+1}.
\end{aligned} \tag{42}$$

The effective lattice model in the s -wave approximation for the Landau function, is depicted in Fig. 11. The even sublattice has one attractive impurity on site $l = 0$. The bonds between the $l = 0$ and $l \pm 1$ sites are chiral ($J' \neq J$), and the bond in the backward direction (from ± 1 to 0) is weak ($J' < J$). If not for the bond defect, the even sublattice would have a single bound state with an even-parity wavefunction. The odd sublattice has two impurities (on sites $l = -1$ and $l = 0$) connected by a weak non-chiral bond. The odd sublattice can have up to two bound states, with even- and odd-parity wavefunctions. As in the case of Rashba SOC plus magnetic field, the maximum number of bound states is three. The difference is that in the Rashba plus field case, two out of the three possible states are “extra” states which are formed only if impurities are sufficiently strong. As impurities get weak (relative to the bandwidth), we loose the extra states one by one. Accordingly, two out of three collective modes in Fig. 5a run into the continuum, while the remaining third mode grazes along the continuum. In the Rashba plus Dresselhaus case, the three bound states come as a singlet from the even sublattice and a doublet from the odd sublattice. Only one of the components of the doublet is an “extra” state, and we should expect this state to run into the continuum. The remaining component of the doublet and the singlet are the lowest energy bound states which can only eliminated by a competition between impurities and bond defects. Therefore, we should expect these to states to graze the continuum and touch it a special point, where Rashba and Dresselhaus SOC's compensate each other. These

into the continuum at some value of Δ_R/Δ_D , while the two lower energy modes graze the continuum and touch it at $\Delta_R = \Delta_D$. The conditions for touching can be derived in the same as it was in the previous section for the Rashba plus field case.

VII. Conclusions

We showed that in FL theory, the system of coupled kinetic equations for the angular harmonics of the distribution function can be mapped onto an effective one-dimensional tight-binding model where the lattice sites correspond to the values of the angular momentum. In this mapping, Rashba term plays the role of on-site energies, Zeeman and Dresselhaus terms are responsible for nearest and next-to-nearest neighbor hopping and the continuum of spin-flip particle hole excitations becomes a lattice band. FL interaction, characterized by the harmonics of the Landau function, produces effective disorder of both on-site and bond type. The collective modes correspond to the bound states produced by this disorder. This mapping is good only when two of the three couplings—Rashba, Dresselhaus and Zeeman—are present, absence of any two would make this theory incomplete. We also claim that our theory is valid for zero sound waves too where the collision integral in the transport equation is omitted because the scattering rate, $1/\tau \propto T^2$ and since in the collisionless limit, the temperature $T \rightarrow 0$, we have $\omega\tau \gg 1$. The resulting equation in the angular space is written as

$$(\omega - v_F^* q \cos \theta) u(\theta) = v_F^* q \cos \theta \int_{\theta'} F^s(\theta') u(\theta'), \tag{43}$$

where v_F^* is the renormalized Fermi velocity and $\int_{\theta'} = \int \frac{d\theta'}{2\pi}$. For the solution of this equation to be analytic we must have $\omega \geq v_F^* q$. Here, $\omega = v_F^* q$ defines the upper boundary of the particle-hole continuum and $\omega > v_F^* q$ leads to zero sound mode. Since this mode is always outside the continuum, it is undamped and long lived. Now, we understand this result in the effective lattice language because, in the case of on-site impurities at sites $m = 0$ and ± 1 , due to no competition with bond disorder, there is always atleast one bound state which is in perfect agreement with the collisionless limit.

The advantage of this work is that it provides the complete picture of many body theory of ESR. The best plat-

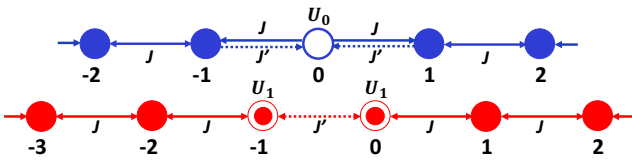


FIG. 11. Effective lattice model for a FL with both Rashba and Dresselhaus spin-orbit couplings in the s -wave approximation.

expectations are indeed confirmed by an exact solution of Eq. (42), which is plotted in Fig. 12. The spectrum is symmetric about the $SU(2)$ -symmetric point, where $\Delta_R = \Delta_D$. On each side of this point, there are up to three collective modes. The highest-energy mode runs

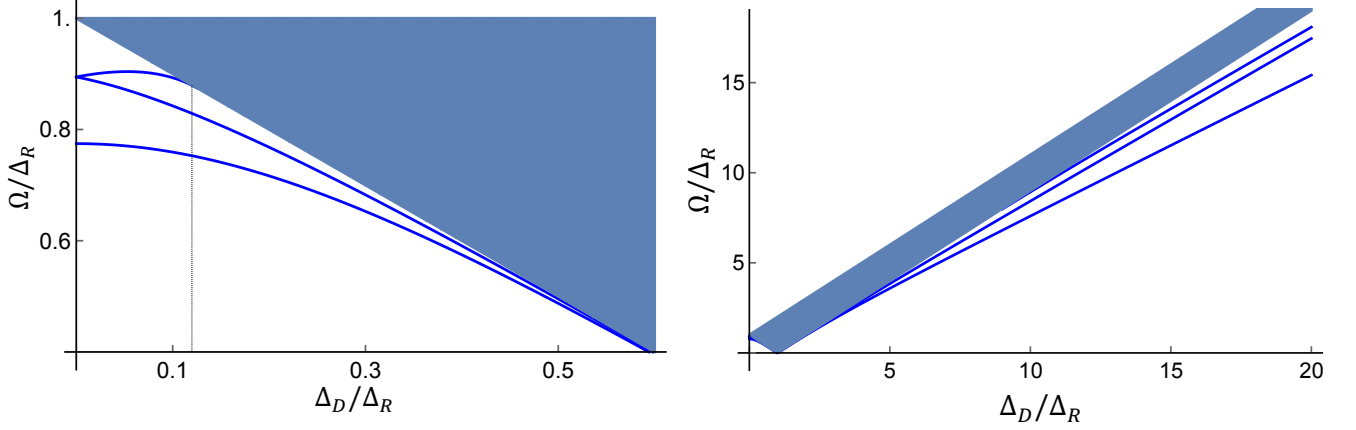


FIG. 12. Collective modes of a FL with Rashba and Dresselhaus spin-orbit couplings. The Landau function is taken in the s -wave approximation with $F_0^a = -0.4$.

form that can host these type of modes is semiconductor heterostructure in the regime when the SOC is comparable to the Zeeman splitting due to an in-plane magnetic field. These can be identified as absorption peaks in ESR spectroscopy.

Acknowledgments

We thank C. Batista, S. Maiti, A. Rustagi, M. Imran, and C. Reeg for stimulating discussions. This work was supported by the National Science Foundation via grant NSF DMR-1308972. D.L.M acknowledges hospitality of the Center for Non-Linear Studies, Los Alamos National Laboratory, which he visited in 2015-2016 as an Ulam Scholar.

A. One-dimensional tight-binding model with impurities and bond defects

In this Appendix we solve a number of one-dimensional tight-binding models with impurities and bond defects, depicted in Fig. 6.

1. On-site disorder

Let us first discuss the case when there is an impurity at site $m = 0$ of a 1D lattice, as shown in Fig ???. We assume that this impurity does not affect its nearest neighbors and they are connected to the impure site through normal bonds like all the other sites to its nearest neighbors. We term this model as *tight-binding with on-site disorder*.

Let ψ_m with $m \in \mathbb{Z}$ be the wavefunction amplitudes at lattice sites. The equations for amplitude at different

sites can be written as

$$E\psi_m = U_0\delta_{m,0}\psi_m - (\psi_{m-1} + \psi_{m+1}), \quad (\text{A1})$$

where E is the particle energy and U_0 is the impurity potential. Since all the connecting bonds are normal and the system is symmetric about site $m = 0$, it is legitimate to make the transformation, $\psi_{\pm(|m|+1)} = e^{-(|m|+1)\lambda}\psi_0$ and get the system of equations in a closed form. Physically this transformation is logical in a sense that the wavefunction, away from the impurity site, must decay exponentially in order to have a bound state. Our goal now is to diagonalize this system and obtain the bound states. The system of equations read

$$\begin{aligned} E\psi_0 &= U_0\psi_0 - (\psi_{-1} + \psi_1), \\ E\psi_{\pm(|m|+1)} &= -(\psi_{\pm|m|} + \psi_{\pm(|m|+2)}). \end{aligned} \quad (\text{A2})$$

The second equation in Eq. (A2) gives the expression of $e^{-\lambda}$ as

$$e^{-\lambda} = -\frac{E}{2} \pm \sqrt{\frac{E^2}{4} - 1}, \quad (\text{A3})$$

which upon substituting in the first equation of Eq. (A2), we obtain $E = \pm\sqrt{U_0^2 + 4}$. We note that these eigenvalues are obtained from the non-linear equation, so the solution is true for only certain range of values of U_0 . For $U_0 < 0$, we have a bound state, $E = -\sqrt{U_0^2 + 4}$, below the bottom of the band and for $U_0 > 0$, a bound state, $E = \sqrt{U_0^2 + 4}$, above the top of the band. This is precisely what we expect from our semiconductor physics that a tight-binding band has both electron states with positive effective mass (with energies below the middle of the band) and hole states with negative effective mass (with energies above the middle of the band). An attractive potential, $U_0 < 0$, binds electrons into states below the bottom of the band and a repulsive potential, $U_0 > 0$ binds holes into states above the top of the band. This is why we have both donors and acceptors in semiconductors. This model is well suited to our original system

in the specific limit when $\Delta_Z^* \gg \Delta_R^*$ for s-wave interaction. There also we have just one spin-collective mode, bound state in tight-binding language, below the continuum for attractive interaction or above the continuum for repulsive interaction.

2. Bond disorder

We consider that due to an impurity at site $m = 0$, only the bonds connecting to its adjacent sites, i.e., $m = \pm 1$ are disordered as shown in Fig. ???. The system of equations for the wavefunction amplitudes can be written as

$$\begin{aligned} E\psi_0 &= -J(\psi_{-1} + \psi_1), \\ E\psi_{\pm 1} &= -J\psi_0 - \psi_{\pm 2}, \\ E\psi_{\pm(|m|+2)} &= -(\psi_{\pm(|m|+1)} + \psi_{\pm(|m|+3)}), \end{aligned} \quad (\text{A4})$$

where $J > 0$ is the overlap integral from sites $m = 0$ to $m = \pm 1$. All the other overlaps in the system are considered normal.

To get the system of equations in the closed form we choose ψ_0 and $\psi_{\pm 1}$ as independent variables and starting from $m = \pm 2$ use the Ansatz $\psi_{\pm(|m|+2)} = e^{-(|m|+1)\lambda}\psi_{\pm 1}$. Here $e^{-\lambda}$ is obtained in the same way as that in the previous section. To simplify the calculation, we set $\psi_0 = 1$ and $\psi_1 = \psi_{-1}$. The eigenvalues of Eq. (A4) are obtained by eliminating ψ_1 in favor of ψ_0 which read

$$E = \pm \frac{2J^2}{\sqrt{2J^2 - 1}}. \quad (\text{A5})$$

Since, this formula is obtained from non-linear equation, it is valid only in certain range of values of J . Upon straightforward algebra, we obtain that $E = -2J^2/\sqrt{2J^2 - 1}$ is the bound state energy with wavefunction, $e^{-\lambda} = -E/2 - \sqrt{E^2/4 - 1}$ for $J > 1$. The bond disorder binds electrons below the bottom of the lattice band with this energy. Similarly, there is another combination of bound state, $E = 2J^2/\sqrt{2J^2 - 1}$ corresponding to the wavefunction $e^{-\lambda} = -E/2 + \sqrt{E^2/4 - 1}$ for $J > 1$, which can be understood as binding of holes by this disorder above the top of the lattice band. So, conclusively we expect to see two bound states—one above and one below the lattice band—for a given $J > 1$ and no bound state for $J < 1$.

To understand the physical picture behind the appearance of bound state, we go to its continuum representation. The difference equation for wavefunction at site $m = 0$ is written as

$$E\psi_0 = -J(\psi_1 + \psi_{-1}). \quad (\text{A6})$$

The continuum representation reads

$$(E + 2J)\psi(x) = -\frac{1}{2m} \frac{d^2\psi(x)}{dx^2} \quad (\text{A7})$$

where $m = 1/2Ja^2$. This equation is nothing but the familiar Schroedinger equation with confining potential well of strength $2J$. The motion is free if $E > -2J$ and the corresponding wavefunction is a simple plane wave. To understand the physical picture, suppose that there is an interface between two materials with the confining potential characterized by J_1 and J_2 to the left and right side of the interface correspondingly. The motion is free in the left material, if $E > -2J_1$, and is confined in the right material, if $E < -2J_2$. This implies that $J_1 > J_2$, in which case an electron propagating from the left is not able to penetrate to the right, and its wavefunction decays exponentially into the material on the right. This means that the bond disorder, like on-site disorder, is also mapped onto the potential step problem in the continuum, see Fig. 8.

The lattice picture in the continuum can now be modeled as a junction consisting of a narrow-gap material $(-\infty, -L/2)$, wide-gap material $(-L/2, L/2)$, and again narrow-gap material $(L/2, \infty)$. An electron is free to move within the wide-gap material, but its wavefunction will decay exponentially in the narrow-gap regions. This is the reason for the condition $J > 1$: it corresponds to having a segment of a wide-gap material. This argument also gives a clear picture that even if there is just one bond disorder (one atomic spacing), for e.g. bond between sites $m = 0$ and $m = 1$ is only defective, the condition for J would remain the same. In semiconductor physics, this is known as “band mismatch”, which occurs at interfaces between different semiconductors.

3. Competition between on-site disorder and bond disorder

To understand how both on-site and bond disorder affects bound states in the system, we discuss the simplest model where in addition to the on-site impurity at site $m = 0$ the bonds connecting to its nearest-neighbors, $m = \pm 1$, are also defective, see Fig. ??. The system of equations for the wavefunction amplitudes read

$$\begin{aligned} E\psi_0 &= -U_0\psi_0 - J(\psi_{-1} + \psi_1), \\ E\psi_{\pm 1} &= -J\psi_0 - \psi_{\pm 2}, \\ E\psi_{\pm(|m|+2)} &= -(\psi_{\pm(|m|+1)} + \psi_{\pm(|m|+3)}), \end{aligned} \quad (\text{A8})$$

where $U_0 > 0$ is the on-site impurity potential and $J > 0$ is the bond disorder strength. Negative sign in front of U_0 ensures that we have considered attractive impurity potential. To simplify our calculation, we set $\psi_0 = 1$ and $\psi_1 = \psi_{-1}$. To get the system of equations in the closed form we use the same Ansatz as above, which is $\psi_{\pm(|m|+2)} = e^{-(|m|+1)\lambda}\psi_{\pm 1}$. We are mainly interested in bound states below the conduction band, so we choose

$$e^{-\lambda} = -\frac{E}{2} - \sqrt{\frac{E^2}{4} - 1}. \quad (\text{A9})$$

Somewhere in the intermediate step of the calculation we obtain

$$U_0 + E(1 - J^2) = 2J^2 \sqrt{\frac{E^2}{4} - 1}, \quad (\text{A10})$$

where $E = -|E|$. More precisely, since the tight-binding band occupies the interval, $-2 \leq E \leq 2$, the bound states below the conduction band obey the condition, $E < -2$ or $|E| > 2$. Eq. (A10) can now be written as

$$U_0 - |E|(1 - J^2) = 2J^2 \sqrt{\frac{E^2}{4} - 1}. \quad (\text{A11})$$

Though one can solve this equation to get energy eigenvalues of the system but that is not we are interested in here. We actually want to find out the algebraic relation between on-site and overlap parameters, upon looking at which one can say with certainty why bound states doesn't exist beyond a critical point.

For $U_0 = 0$, there is a bound state if $J^2 > 1$. We know this from the slope of the curves of expressions on the LHS and RHS. Slope of the expression on LHS is smaller as compared to that on the RHS in the limit $E \gg 1$. It means that the curves must have intersected each other at some point which signals a solution of Eq. (A11) which lies below the conduction band. For $J^2 < 1$, the slope on the LHS is negative whereas it is still positive on the RHS. It shows that there is no bound state. This is what we expect from our previous section's result also. Now, for $U_0 \neq 0$ and $J^2 > 1$, by the same argument of slopes, there is always a solution. The attractive impurity and $J^2 > 1$ help each other. For $U_0 \neq 0$ but $J^2 < 1$, solution is possible only if $U_0 - 2(1 - J^2) > 0$. If $U_0 > 2$, this condition is always satisfied but if $U_0 < 2$, there is a critical value

$$J_c^2 = 1 - \frac{U_0}{2} \quad (\text{A12})$$

below which bound state disappears. So, we conclude that if $U_0 > 2$, there is always a bound state below the conduction band for all $J > 0$, and if $U_0 < 2$, there is no bound state for $J^2 < 1 - U_0/2$.

4. Competition between three on-site impurities and two defect bonds

We consider slightly more complicated model where the competition between on-site disorder and bond disorder is understood more clearly by realizing the transition of number of bound states from 3 to 2 to finally 1. To understand this effect, we consider that there are three on-site impurities of same strength at sites $m = 0$ and ± 1 and the bonds connecting them are defective, see Fig. 13.

The system is described by the following set of equa-

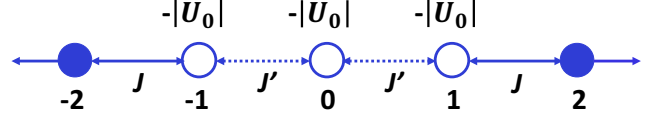


FIG. 13. One-dimensional tight-binding model with three on-site attractive impurities at sites $m = 0$ and ± 1 . The bond connecting them are defect bonds with amplitude J . All the other bonds are normal, i.e., $J' = 1$.

tions,

$$\begin{aligned} E\psi_0 &= -U_0\psi_0 - J(\psi_{-1} + \psi_1), \\ E\psi_{\pm 1} &= -U_0\psi_{\pm 1} - J\psi_0 - \psi_{\pm 2}, \\ E\psi_{\pm(|m|+2)} &= -(\psi_{\pm(|m|+1)} + \psi_{\pm(|m|+3)}), \end{aligned} \quad (\text{A13})$$

where all the parameters have their usual meaning. We get the system of equations in the closed form by using the same Ansatz as considered in the previous sections of this Appendix. Since the impurity is attractive in nature, we choose $e^{-\lambda}$ same as that in Eq. (A9). Here, it is not helpful to eliminate ψ_1 in favor of ψ_0 because in the process, we will lose information of one bound state. So, it is better to write the equations corresponding to lattice sites $m = 0$ and ± 1 in the matrix form as was written in Eq. (33) of the main text. For non-trivial solution, we set the determinant of 3×3 matrix to 0 and obtain the equation as

$$\{E + U_0 + e^{-\lambda}\} \{(E + U_0)(E + U_0 + e^{-\lambda}) - 2J^2\} = 0. \quad (\text{A14})$$

We set each bracketed term to 0 and look for the effects of U_0 and J^2 on bound states. From

$$E + U_0 + e^{-\lambda} = 0 \quad (\text{A15})$$

we obtain $E = -U_0 - 1/U_0$ which is valid for $U_0 > 1$. This equation does not have any competition between on-site and overlap parameters, so we do not need to worry about this. Upon substituting Eq. (A9) in

$$(E + U_0)(E + U_0 + e^{-\lambda}) - 2J^2 = 0, \quad (\text{A16})$$

and for $E = -|E|$, we obtain

$$(E - U_0)(E - U_0 + e^{-\lambda}) - 2J^2 = 0, \quad (\text{A17a})$$

$$E - U_0 + e^{-\lambda} = 0, \quad (\text{A17b})$$

correspondingly. Equation (A17b) yields $E = U_0 + 1/U_0$, which satisfies the condition of the bound state to be below the band edge, i.e., $E < -2$, for $U_0 < -1$. Since the odd-parity eigenvalue does not depend on J' , it is not affected by the competition between on-site and bond defects. Equation (A17a) for the even-parity eigenvalue is reduced to

$$\frac{E^2}{2} - \frac{3}{2}EU_0 + U_0^2 - 2J^2 = (E - U_0)\sqrt{\frac{E^2}{4} - 1}. \quad (\text{A18})$$

DM: give more details for the argument till the end of the section

To find out the solution of the above equation, we use the same argument as that for three attractive impurities case. The bound states are below the band edge for $E < -2$ which leads to the RHS of Eq. (A18) negative-definite for $-2 < U_0 < 0$. At $E = -2$, the LHS is $P = U_0^2 + 3U_0 + 2 - 2J^2$. For $-2 < U_0 < 0$ and $2J^2 > U_0^2 + 3U_0 + 2$, P is negative and Eq. (A18) has only one root. If $U_0 < -2$, the RHS of Eq. (A18) vanishes at $E = -2$ and $E = U_0$, and has a maximum in between these two points. For $2J^2 > U_0^2 + 3U_0 + 2$, the LHS is still negative and thus the equation has only one root. For the case when $U_0 < -2$ and $0 < 2J^2 < U_0^2 + 3U_0 + 2$, the equation has two roots. Now combining all these arguments with the odd-parity case, we conclude that for $-1 < U_0 < 0$ and $2J^2 >$

$U_0^2 + 3U_0 + 2$, the system has only one bound state which increases to two for $U_0 < -1$ and $2J^2 > U_0^2 + 3U_0 + 2$. There are three bound states when $U_0 < -1$ and $0 < 2J^2 < U_0^2 + 3U_0 + 2$.

B. Collective modes for interaction in $m = 0$ channel within tight-binding formalism

In this Appendix, we provide explicitly the expression of collective modes for interaction in $m = 0$ angular harmonic channel obtained within tight-binding formalism. Equating the determinant of 3×3 matrix in Eq. (33) to zero, we get the collective mode frequencies which read

$$\begin{aligned}
\Omega_1^2 &= \left[1 + \frac{F_0^a}{2}\right] \Delta_R^2 + \left[1 + \frac{2}{F_0^a}\right] \Delta_Z^{*2}, \\
\Omega_2^2 &= P + \frac{1}{3 \times 2^{2/3}} \frac{1}{F_0^a} \left[\frac{Q}{(\text{Re}\{Z\})^2 + (\text{Im}\{Z\})^2} - 2^{-2/3} \right] \text{Re}\{Z\}, \\
\Omega_3^2 &= P - \frac{1}{6 \times 2^{2/3}} \frac{1}{F_0^a} \left[\frac{Q}{(\text{Re}\{Z\})^2 + (\text{Im}\{Z\})^2} - 2^{-2/3} \right] [\text{Re}\{Z\} + \sqrt{3} \text{Im}\{Z\}], \\
\text{where, } Z &= \left(R + \sqrt{4Q^3 + R^2}\right)^{1/3} \text{ and} \\
P &= \frac{1}{6} \left[6 + 5F_0^a\right] \Delta_R^2 - \frac{1}{3F_0^a} \left[2 + 5F_0^a + (F_0^a)^2 - (F_0^a)^3\right] \Delta_Z^{*2} \\
Q &= - (F_0^a)^4 \Delta_R^4 - 4(F_0^a)^2 \left[2 + 8F_0^a + 7(F_0^a)^2 + 2(F_0^a)^3\right] \Delta_R^2 \Delta_Z^{*2} - 4 \left[4 + 32F_0^a + 68(F_0^a)^2 + 60(F_0^a)^3 + 27(F_0^a)^4\right. \\
&\quad \left.+ 7(F_0^a)^5 + (F_0^a)^6\right] \Delta_Z^{*4} \\
R &= 2(F_0^a)^6 \Delta_R^6 + 12(F_0^a)^4 \left[2 + 8F_0^a + 7(F_0^a)^2 + 2(F_0^a)^3\right] \Delta_R^4 \Delta_Z^{*2} - 12(F_0^a)^2 \left[136 + 512F_0^a + 776(F_0^a)^2 + 612(F_0^a)^3\right. \\
&\quad \left.+ 261(F_0^a)^4 + 55(F_0^a)^5 + 4(F_0^a)^6\right] \Delta_R^2 \Delta_Z^{*4} + 8 \left[16 + 192F_0^a + 792(F_0^a)^2 + 1480(F_0^a)^3 + 1392(F_0^a)^4 + 630(F_0^a)^5\right. \\
&\quad \left.+ 62(F_0^a)^6 - 57(F_0^a)^7 - 21(F_0^a)^8 - 2(F_0^a)^9\right] \Delta_Z^{*6}
\end{aligned} \tag{B1}$$

These solutions are plotted in Fig. 5 as a function of increasing magnetic field. The above formula for collective modes is true only until it touches the continuum, the extended tail is not a part of the solution. The reason is that these modes are obtained from non-linear equation which doesn't give exact solutions, it has solution only in the certain range of parameter values.

C. Interaction in $m = 0$ and $m = 1$ harmonic channel

In this Appendix, we provide the details to determine collective modes of two-dimensional electron system with Rashba SOC in the presence of in-plane magnetic field within FL theory for interaction in $m = 0$ and $m = 1$ angular harmonic channels using tight-binding formalism. This is understood by considering $F^a(\theta_{pp'}) = F_{-1}^a e^{-i\theta_{pp'}} + F_0^a + F_1^a e^{i\theta_{pp'}}$, where F_i^a are the Landau interaction parameters in i^{th} harmonic channel, in Eqs. (11a) - (11c). We use the same transformation, $\psi_m \equiv i^{-m} u_1^m$ as that in for s-wave in the second order time-derivative equation for u_1^m and obtain the complete form as

$$\begin{aligned}
-\Omega^2 i^m \psi_m = & -i^m \left(\Delta_R^{*2} + \Delta_Z^{*2} \right) \psi_m + i^m \Delta_R^* \Delta_Z^* \left(\psi_{m-1} + \psi_{m+1} \right) + F_{-1}^a \left\{ -\frac{1}{2} \Delta_R^{*2} (1 + F_0^a) \psi_0 + \frac{1}{2} \Delta_R^* \Delta_Z^* (3 + F_{-1}^a) \psi_{-1} \right\} \delta_{m,0} \\
& + F_0^a \left\{ -\left(\Delta_R^{*2} + (2 + F_0^a) \Delta_Z^{*2} \right) \psi_0 + \frac{1}{2} \Delta_R^* \Delta_Z^* (1 + F_{-1}^a) \psi_{-1} + \frac{1}{2} \Delta_R^* \Delta_Z^* (1 + F_1^a) \psi_1 \right\} \delta_{m,0} \\
& + F_1^a \left\{ -\frac{1}{2} \Delta_R^{*2} (1 + F_0^a) \psi_0 + \frac{1}{2} \Delta_R^* \Delta_Z^* (3 + F_1^a) \psi_1 \right\} \delta_{m,0} \\
& + F_{-1}^a \left\{ -\frac{i}{2} \Delta_R^* \Delta_Z^* \psi_{-2} + i \left(\Delta_R^{*2} + (2 + F_{-1}^a) \Delta_Z^{*2} \right) \psi_{-1} - \frac{i}{2} \Delta_R^* \Delta_Z^* (1 + F_0^a) \psi_0 \right\} \delta_{m,-1} \\
& + F_0^a \left\{ \frac{i}{2} \Delta_R^{*2} (1 + F_{-1}^a) \psi_{-1} - \frac{i}{2} \Delta_R^* \Delta_Z^* (3 + F_0^a) \psi_0 \right\} \delta_{m,-1} \\
& + F_1^a \left\{ \frac{i}{2} \Delta_R^* \Delta_Z^* \psi_2 - i \left(\Delta_R^{*2} + (2 + F_1^a) \Delta_Z^{*2} \right) \psi_1 + \frac{i}{2} \Delta_R^* \Delta_Z^* (1 + F_0^a) \psi_0 \right\} \delta_{m,1} \\
& + F_0^a \left\{ -\frac{i}{2} \Delta_R^{*2} (1 + F_1^a) \psi_1 + \frac{i}{2} \Delta_R^* \Delta_Z^* (3 + F_0^a) \psi_0 \right\} \delta_{m,1} \\
& + F_{-1}^a \left\{ \frac{1}{2} \Delta_R^{*2} \psi_{-2} - \frac{1}{2} \Delta_R^* \Delta_Z^* (1 + F_{-1}^a) \psi_{-1} \right\} \delta_{m,-2} + F_1^a \left\{ \frac{1}{2} \Delta_R^{*2} \psi_2 - \frac{1}{2} \Delta_R^* \Delta_Z^* (3 + F_1^a) \psi_1 \right\} \delta_{m,2}.
\end{aligned} \tag{C1}$$

Here $F_{-1}^a = F_1^a$, because the harmonic coefficients are even in m . We write the above system of equations for

different harmonics to realize it on a 1D effective lattice. The system of equations read

$$\begin{aligned}
-\Omega^2 \psi_0 = & -\left[\Delta_R^{*2} (1 + F_1^a) (1 + F_0^a) + \Delta_Z^{*2} (1 + F_0^a (2 + F_0^a)) \right] \psi_0 + \Delta_R^* \Delta_Z^* \left[1 + \frac{1}{2} F_1^a (3 + F_1^a) + \frac{1}{2} F_0^a (1 + F_1^a) \right] (\psi_{-1} + \psi_1), \\
-\Omega^2 \psi_{\pm 1} = & -\left[\Delta_R^{*2} (1 + F_1^a) (1 + \frac{1}{2} F_0^a) + \Delta_Z^{*2} (1 + F_1^a (2 + F_1^a)) \right] \psi_{\pm 1} + \Delta_R^* \Delta_Z^* \left[1 + \frac{1}{2} F_1^a (1 + F_0^a) + \frac{1}{2} F_0^a (3 + F_0^a) \right] \psi_0 \\
& + \Delta_R^* \Delta_Z^* \left[1 + \frac{1}{2} F_1^a \right] \psi_{\pm 2}, \\
-\Omega^2 \psi_{\pm 2} = & -\left[\Delta_R^{*2} \left(1 + \frac{1}{2} F_1^a \right) + \Delta_Z^{*2} \right] \psi_{\pm 2} + \Delta_R^* \Delta_Z^* \left[1 + \frac{1}{2} F_1^a (3 + F_1^a) \right] \psi_{\pm 1} + \Delta_R^* \Delta_Z^* \psi_{\pm 3}, \\
-\Omega^2 \psi_{\pm(|m|+3)} = & -\left[\Delta_R^{*2} + \Delta_Z^{*2} \right] \psi_{\pm(|m|+3)} + \Delta_R^* \Delta_Z^* (\psi_{\pm(|m|+2)} + \psi_{\pm(|m|+4)}).
\end{aligned} \tag{C2}$$

We make the transformation, $\psi_{\pm(|m|+3)} = e^{-(|m|+1)\lambda} \psi_{\pm 2} \forall m \geq 0$ to close the system. Here $e^{-\lambda}$ takes the same form as that mentioned in Sec. VC of the main text. We make another transformation, $\psi_{\pm 2} = e^{-\lambda_1} \psi_{\pm 1}$ to project $\psi_{\pm 2}$ on $\psi_{\pm 1}$ and reduce the resulting 5×5 system to 3×3 , where

Finally, this 3×3 system is written in a matrix form as

$$e^{-\lambda_1} = \frac{\Delta_R^* \Delta_Z^* \left(1 + \frac{1}{2} F_1^a (3 + F_1^a) \right)}{(\Delta_R^{*2} + \Delta_Z^{*2} - \Omega^2) - \Delta_R^* \Delta_Z^* e^{-\lambda} + \frac{1}{2} \Delta_R^{*2} F_1^a}. \tag{C3}$$

$$\begin{bmatrix} F_{11}(\Omega) & F_{12}(\Omega) & 0 \\ F_{21}(\Omega) & F_{22}(\Omega) & F_{23}(\Omega) \\ 0 & F_{32}(\Omega) & F_{33}(\Omega) \end{bmatrix} \begin{bmatrix} \bar{v}_{-1} \\ \bar{v}_0 \\ \bar{v}_1 \end{bmatrix} = \begin{bmatrix} 0 \\ 0 \\ 0 \end{bmatrix},$$

$$\text{where, } F_{11}(\Omega) = F_{33}(\Omega) = \Omega^2 - \left[\Delta_R^{*2}(1 + F_1^a)(1 + \frac{1}{2}F_0^a) + \Delta_Z^{*2}(1 + F_1^a(2 + F_1^a)) \right] + \Lambda,$$

$$F_{12}(\Omega) = F_{32}(\Omega) = \Delta_R^* \Delta_Z^* \left[1 + \frac{1}{2}F_1^a(1 + F_0^a) + \frac{1}{2}F_0^a(3 + F_0^a) \right], \quad (\text{C4})$$

$$F_{21}(\Omega) = F_{23}(\Omega) = \Delta_R^* \Delta_Z^* \left[1 + \frac{1}{2}F_1^a(3 + F_1^a) + \frac{1}{2}F_0^a(1 + F_1^a) \right],$$

$$F_{22}(\Omega) = \Omega^2 - \left[\Delta_R^{*2}(1 + F_1^a)(1 + F_0^a) + \Delta_Z^{*2}(1 + F_0^a(2 + F_0^a)) \right],$$

$$\text{and } \Lambda = \frac{2\Delta_R^{*2}\Delta_Z^{*2}(1 + \frac{1}{2}F_1^a)(1 + \frac{1}{2}F_1^a(3 + F_1^a))}{(\Delta_R^{*2} + \Delta_Z^{*2} - \Omega^2) + \Delta_R^{*2}F_1^a + \sqrt{(\Delta_R^{*2} + \Delta_Z^{*2} - \Omega^2)^2 - 4\Delta_R^{*2}\Delta_Z^{*2}}}.$$

The determinant of 3×3 matrix equated to zero gives the collective modes of the system. It can be seen that for

$F_1^a = 0$, the matrix equation goes back to our s -wave case.

* kumarabhi@ufl.edu; corresponding author

- ¹ S. Datta and B. Das, *Applied Physics Letters* **56**, 665 (1990).
- ² H. L. Stormer, Z. Schlesinger, A. Chang, D. C. Tsui, A. C. Gossard, and W. Wiegmann, *Phys. Rev. Lett.* **51**, 126 (1983).
- ³ D. Stein, K. v. Klitzing, and G. Weimann, *Phys. Rev. Lett.* **51**, 130 (1983).
- ⁴ Z. Wilamowski, H. Malissa, F. Schäffler, and W. Jantsch, *Phys. Rev. Lett.* **98**, 187203 (2007).
- ⁵ R. Winkler, *Spin-Orbit Coupling Effects in Two-Dimensional Electron and Hole Systems* (Springer, Berlin, 2003).
- ⁶ E. I. Rashba and A. L. Efros, *Applied Physics Letters* **83**, 5295 (2003).
- ⁷ A. L. Efros and E. I. Rashba, *Phys. Rev. B* **73**, 165325 (2006).
- ⁸ M. Duckheim and D. Loss, *Nat. Phys* **2**, 195 (2006).
- ⁹ S. Maiti, M. Imran, and D. L. Maslov, *Phys. Rev. B* **93**, 045134 (2016).
- ¹⁰ V. P. Silin, *Sov. Phys. JETP* **6**, 945 (1958).
- ¹¹ A. J. Leggett, *Journal of Physics C: Solid State Physics* **3**, 448 (1970).
- ¹² E. I. Rashba, *Sov. Phys. Solid State* **2**, 1109 (1960).
- ¹³ Y. A. Bychkov and E. Rashba, *JETP Lett.* **39**, 78 (1984).
- ¹⁴ G. Dresselhaus, *Phys. Rev.* **100**, 580 (1955).
- ¹⁵ A. Shekhter, M. Khodas, and A. M. Finkel'stein, *Phys. Rev. B* **71**, 165329 (2005).
- ¹⁶ A. Ashrafi and D. L. Maslov, *Phys. Rev. Lett.* **109**, 227201 (2012).
- ¹⁷ G.-H. Chen and M. E. Raikh, *Phys. Rev. B* **60**, 4826 (1999).

- ¹⁸ In the absence of both types of SOC, the system (12a-12a) does not look like a familiar set of macroscopic equations for the Silin-Leggett mode.^{11,19,20} The difference, however, is superficial and can be removed by rotating the basis of Pauli matrices. As shown in Sec.???, the eigenmode frequencies coincide with the known results.
- ¹⁹ E. M. Lifshitz and L. P. Pitaevskii, *Statistical Physics: Theory of the Condensed State (Course of Theoretical Physics Vol. 9)* (Butterworth-Heinemann, Burlington, 1980).
- ²⁰ G. Baym and C. Pethick, *Landau Fermi-liquid theory: concepts and applications* (John Wiley & Sons, 2008).
- ²¹ S. Maiti, V. Zyuzin, and D. L. Maslov, *Phys. Rev. B* **91**, 035106 (2015).
- ²² S.-S. Zhang, X.-L. Yu, J. Ye, and W.-M. Liu, *Phys. Rev. A* **87**, 063623 (2013).
- ²³ S. Maiti and D. L. Maslov, *Phys. Rev. Lett.* **114**, 156803 (2015).
- ²⁴ If one accounts for $\mathcal{O}(\alpha^2)$ effects, the continuum acquires a finite width proportional to the Rashba energy but, as we mentioned before, such effects are neglected here.
- ²⁵ One could equally well view Eq. (21) as describing a harmonic chain, but the relation between the coefficients of the diagonal and off-diagonal terms is not the same as for the standard case. This can be fixed by attaching each "atom" not only to its nearest neighbors but also to its own site by a spring with a different spring constant. On the other hand, the tight-binding interpretation of this equation is straightforward.
- ²⁶ C. Kittel, *Introduction to Solid State Physics, 8th Edition*. (Wiley, New York, 2005).
- ²⁷ F. T. Vasko and A. V. Kuznetsov, *Electronic states and optical transitions in semiconductor heterostructures* (Springer Science & Business Media, 2012).